# On the Subtropical Edge of the Stratospheric Surf Zone

L. M. POLVANI

*Department of Applied Physics, Columbia University, New York, New York*

D. W. WAUGH AND R. ALAN PLUMB

*Center for Meteorology and Physical Oceanography, Massachusetts Institute of Technology, Cambridge, Massachusetts*

(Manuscript received 22 November 1993, in final form 14 August 1994)

ABSTRACT

The formation of a subtropical "transport barrier" in the wintertime stratosphere is investigated in the context of a high-resolution shallow-water model in which Rossby waves are topographically forced on a zonally symmetric basic state. Two sets of experiments are performed: in the first "adiabatic" set, no dissipation or forcing of the mean state is imposed; in the second set, the layer thickness is relaxed to an equilibrium state taken to be representative of middle stratospheric radiative equilibrium temperatures. It is found that in the adiabatic case only a very weak subtropical barrier forms for forcing amplitudes that generate realistically steep potential vorticity gradients at the edge of the polar vortex; the vigorous wave breaking in the surf zone generates secondary waves that spread and, in turn, break well into the summer hemisphere. In contrast, the inclusion of relaxation to a realistic thermal equilibrium leads to the formation of a subtropical region of steep PV gradients. The strong subtropical shear induced by the diabatic relaxation is shown to be an important factor for the formation of the subtropical edge of the surf zone. Furthermore, the authors demonstrate that a simple one-layer shallow-water model can capture the full process of the formation of a surf zone with both polar and tropical edges starting from conditions typical of the early fall—that is, with a flow in which the polar vortex is not initially present. Finally, the authors quantify the mixing of polar and subtropical air into the midlatitude surf zone with the help of the contour advection technique. Although the quantitative estimates depend sensitively on how the edges of the surf zone are defined, our results indicate that more tropical than polar air is entrained into the surf zone.

## 1. Introduction

It is now well established that in the wintertime stratosphere the polar vortex is surrounded by what McIntyre and Palmer (1983, 1984) have named a "surf zone." The poleward edge of this surf zone, which marks the edge of the polar vortex, is distinguished by steep isentropic gradients in potential vorticity (PV); the formation and development of this "PV barrier" has been the subject of much recent work (for a recent review, see McIntyre 1992). Much less attention, in contrast, has been given to the equatorward edge of the surf zone, although the observations indicate the existence of at least a partial barrier to transport in the subtropical stratosphere and the occurrence of sporadic "wave breaking" events that mix subtropical air poleward into the midlatitude surf zone.

The most direct evidence of the weak transport out of the tropics comes from the longevity (two years or more) of tropical maxima in the concentration of debris from atmospheric nuclear tests (Feely and Spar 1960) and of aerosol produced by tropical volcanic eruptions (e.g., Dyer and Hicks 1968; Trepte and Hitchman 1992). Satellite and airborne lidar observations after the recent eruption of Mt. Pinatubo, in particular, have shown the tropical confinement of the volcanic aerosol, with a sharp edge in the subtropics (e.g., McCormick and Veiga 1992; Read et al. 1993; Trepte et al. 1993; Grant et al. 1994), strongly suggesting the presence of a barrier to transport there. Strong gradients in the tropical regions are also found in in situ aircraft measurements of the ratio of reactive nitrogen and ozone (Murphy et al. 1993).

Furthermore, the satellite observations show poleward transport occurring in narrow "tongues" drawn out of the subtropics into the midlatitudes. Strong gradients in the subtropics and tongues of tropical air are observed in satellite measurements of tracers in the middle and upper stratosphere (Leovy et al. 1985; Randel et al. 1993; Manney et al. 1993). Poleward transport from the subtropics has been reproduced in contour advection calculations using balanced winds from stratospheric analyses (Waugh 1993b) and in tracer simulations with

*Corresponding author address:* Dr. Lorenzo M. Polvani, Department of Applied Physics, Columbia University, Seeley W. Mudd Bldg., Rm. 209, New York, NY 10027.

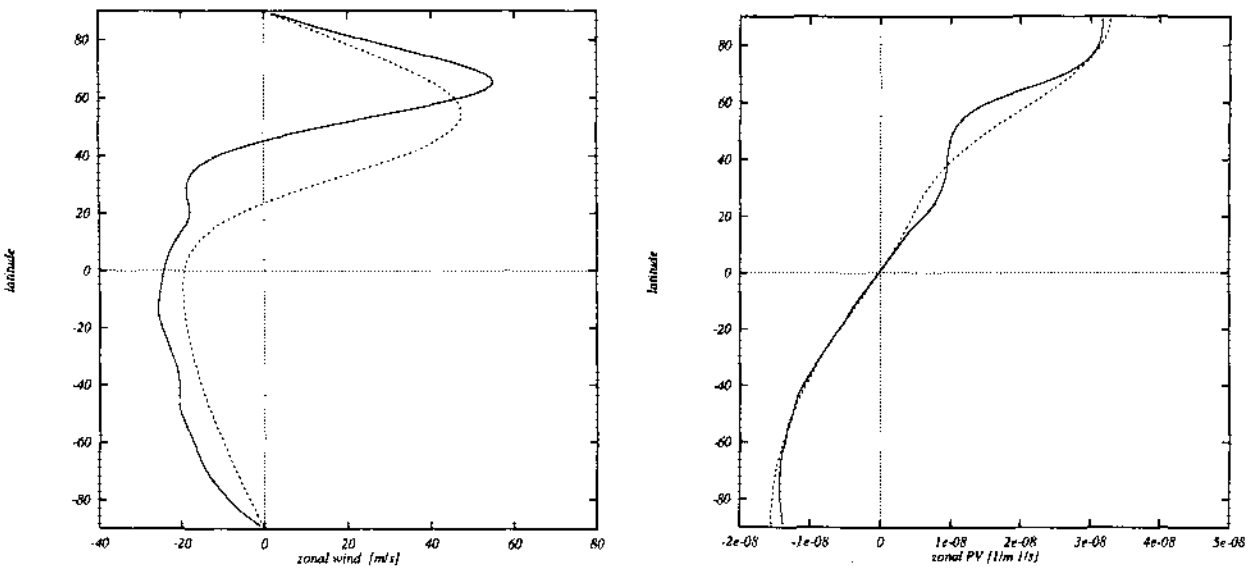


FIG. 1. Zonally averaged (a) wind and (b) potential vorticity profiles at $t = 0$ (dashed) and $t = 100$ days (solid). Notice the formation of a steep PV gradient at the edge of the polar vortex and the absence of a steepening of the PV gradient in the subtropics.

stratospheric general circulation models (Mahlman 1985; Boville et al. 1991; Pierce et al. 1993).

To the best of our knowledge, previous one-layer studies of stratospheric dynamics (Juckes and McIntyre 1987; Juckes 1989; Salby et al. 1990a,b,c; O'Sullivan and Salby 1990; Waugh 1993a; Yoden and Ishioka 1993) have not focused on the issue of a subtropical edge to the surf zone. Recently, Norton (1994) showed the existence of a subtropical edge to the surf zone and poleward wave breaking in his global shallow-water simulations. However, the mechanisms that control the properties of this edge and wave breaking in the subtropics remain to be elucidated.

In this paper, we specifically address the question of the formation of the subtropical edge to the stratospheric surf zone and the transport of subtropical air into and out of the surf zone via planetary wave breaking. We do this by studying the dynamics of a shallow-water model at high resolution, under a range of circumstances. We consider first (section 3) the adiabatic, inviscid response to topographic forcing of a flow initially typical of the winter stratosphere and find that, for forcing amplitudes that produce realistic tightening of PV gradients around the polar vortex, the breaking region extends well beyond the main surf zone, in fact, all the way into the high latitudes of the summer hemisphere. While a main surf zone can be identified in the midlatitudes, its subtropical edge is indistinct and wave breaking occurs both ways across that edge. We next describe experiments that include diabatic relaxation to a state typical of the computed radiative equilibrium state of the stratosphere (section 4). In these experiments, a steep PV gradient forms on the equatorial side of the surf zone, with no apparent equatorward transfer of air across it (i.e., a subtropical transport barrier). In section 5 we discuss experiments in which a surf zone is formed by the combined effect of wave forcing and thermal relaxation from initial conditions approximating those of early autumn. Contour advection calculations are used in section 6 to quantify transport into the surf zone from both the polar vortex and the tropics in these. A summary and discussion of the key results and their implications can be found in section 7.

## 2. The model

We study the flow of a one-layer incompressible fluid on the surface of the sphere obeying the shallow-water equations

$$\begin{aligned}
\zeta_t &= -\nabla\cdot(\mathbf{v}\zeta_a)\\
\delta_t &= -\frac{1}{2}\nabla^2(\mathbf{v}\cdot\mathbf{v}) + \mathbf{k}\cdot\nabla\times(\mathbf{v}\zeta_a) - g\nabla^2(h + h_B)\\
h_t &= -\nabla\cdot(h\mathbf{v}) - \tau_E^{-1}(h - h_E),
\end{aligned} \tag{1}$$

where $\zeta$, $\delta$, and $h$ are the vorticity, divergence, and layer thickness; $\zeta_a$ is the absolute vorticity, defined by $\zeta_a \equiv \zeta + f$ ($f$ is the Coriolis parameter); $\mathbf{v} = (u, v)$ is the velocity; and $h_B$ is the height of the bottom topography [see Eq. (3)]. The last term in the third equation crudely represents the thermal relaxation process (see section 4) by relaxing the fluid depth to an equilibrium distribution $h_E$, with an $e$-folding time $\tau_E$.

In all the calculations we initialize with a zonally symmetric state. Once a zonal flow is specified, $h$ is obtained by numerically integrating the balance equation

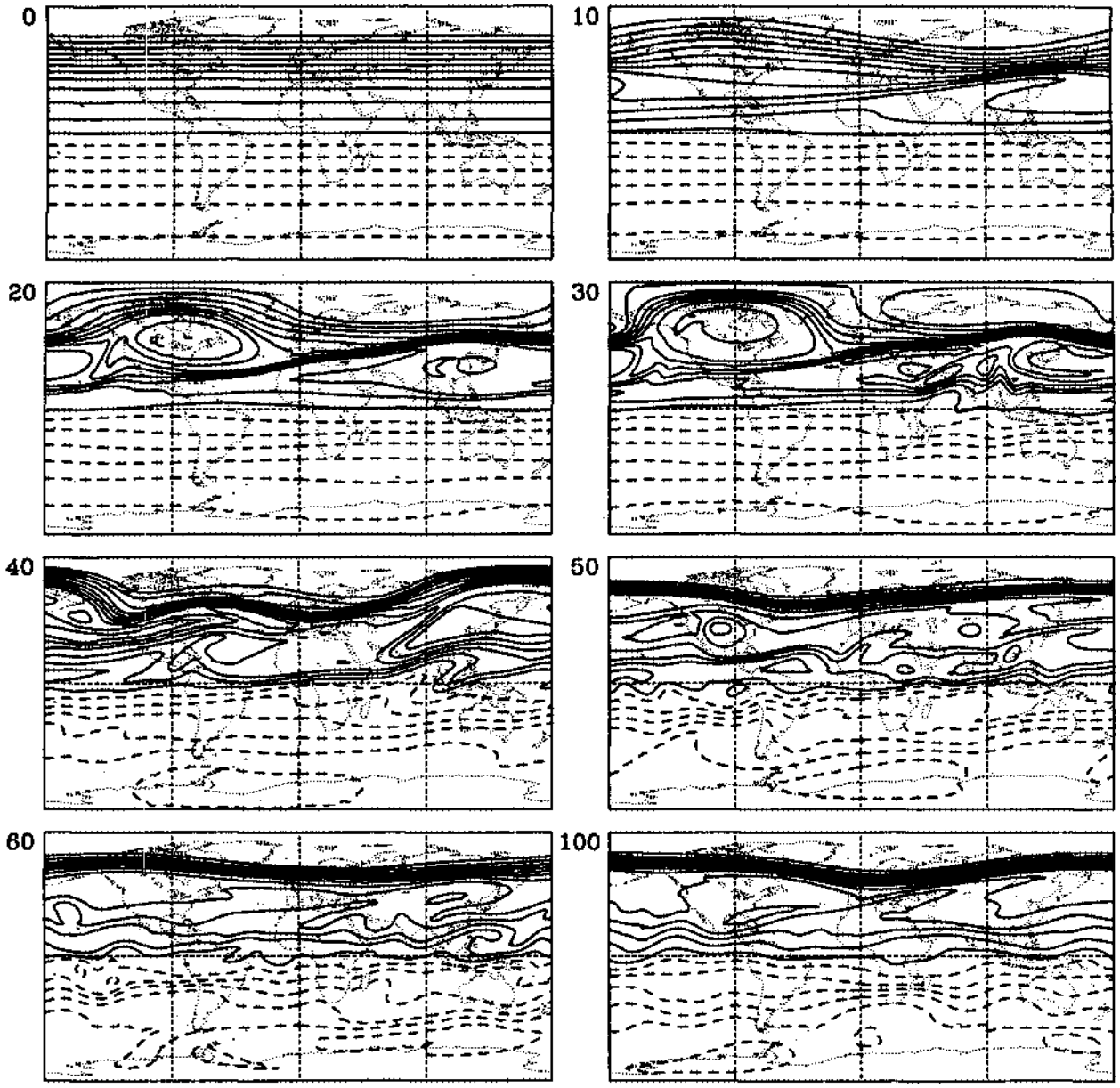


FIG. 2. The response of a polar vortex to topographic forcing in the absence of thermal relaxation. Contours show the potential vorticity in intervals of $0.25 \times 10^{-8}$ m$^{-1}$ s$^{-1}$; negative values are dashed. Time, in days, is in the upper left-hand corner of the maps. This is a cylindrical longitude/latitude projection; 0° of longitude corresponds to the center of the frame. Notice the familiar steepening of the gradients around the polar vortex, and the breaking in the surf zone that extends all the way into the Southern Hemisphere.

$$gh(\varphi) = gh_0 - \int^{\varphi} au(\varphi')\left(f + \frac{\tan\varphi'}{a}u(\varphi')\right)d\varphi', \tag{2}$$

where $u(\varphi)$ is the zonal wind, $\varphi$ indicates latitude, and $a$ is the radius of the earth. Throughout the paper, we have chosen the constant $h_0$ so that the global mean layer thickness is equal to 8 km.

This zonal flow is perturbed by topographic forcing $h_B$ of the form

$$h_B(\varphi, \lambda, t) = H_B T(t)\Phi(\varphi)\cos(\lambda), \tag{3}$$

where $T(t) = 1 - e^{-t/\tau}$, $\Phi(\varphi) = e^{-|(\varphi-\varphi_0)/\Delta\varphi|^2}$, $H_B$ is a constant amplitude, and $\lambda$ is longitude. The topography generates a stationary Rossby wave of zonal wavenumber 1. The time dependence $T(t)$ allows the

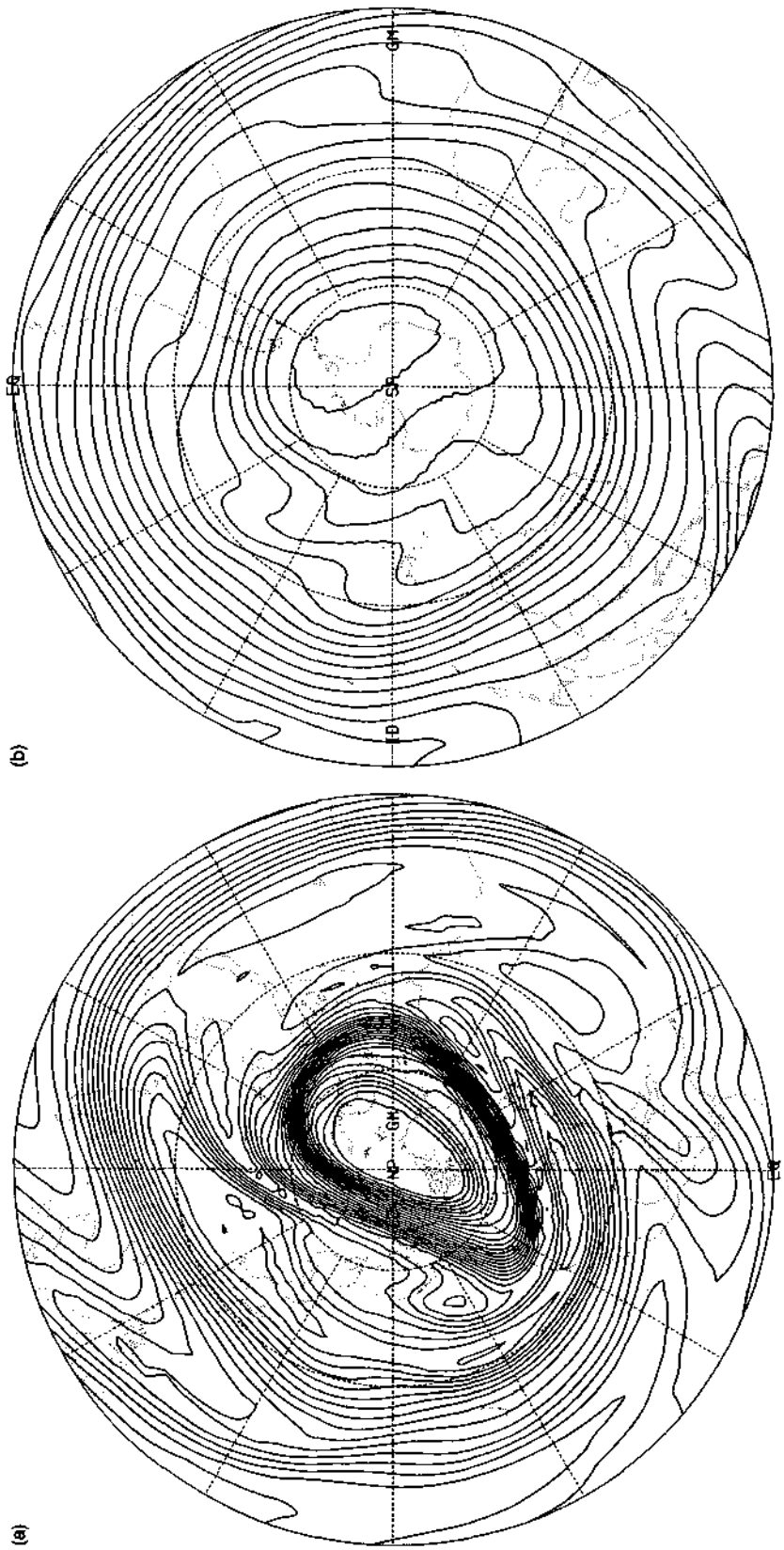


FIG. 3. Polar stereographic views of the PV on day 40 in Fig. 2 for (a) the Northern Hemisphere and (b) the Southern Hemisphere. The contour interval is $0.10 \times 10^{-8}$ m$^{-1}$ s$^{-1}$.

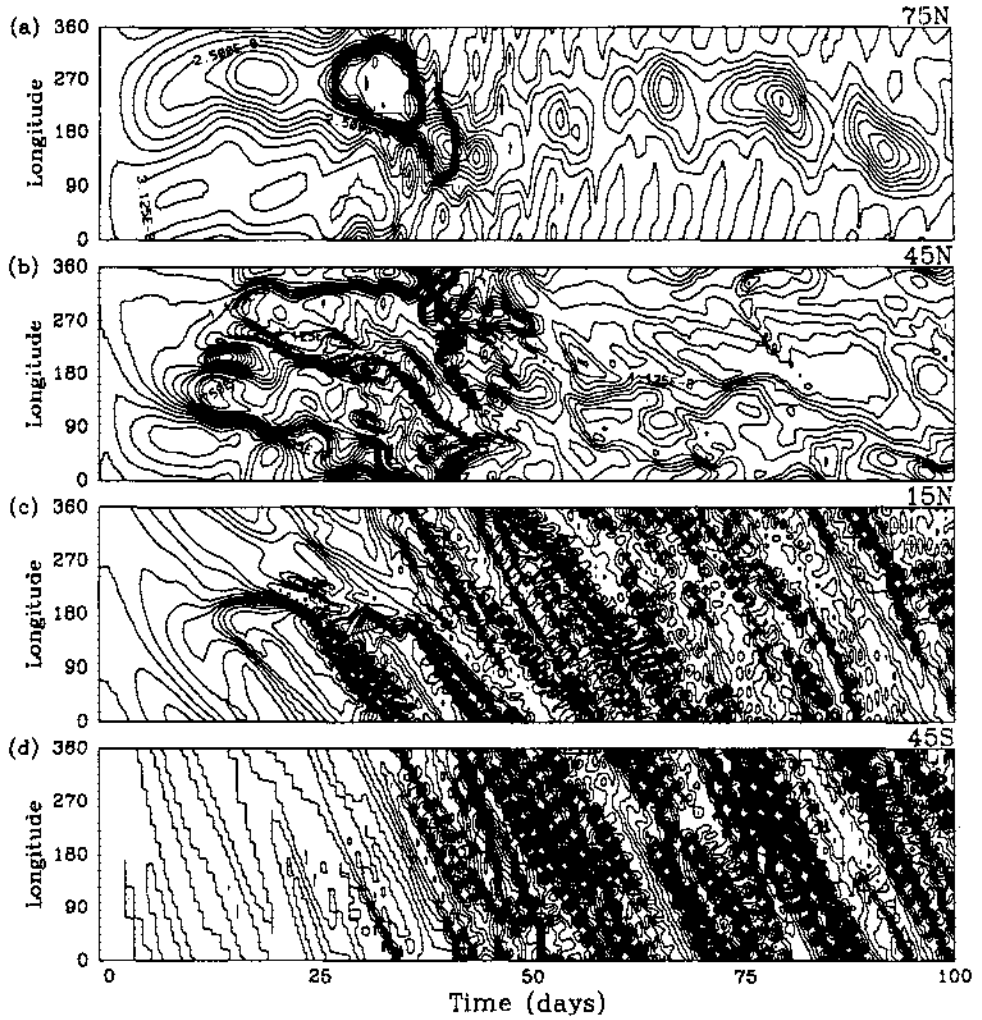


FIG. 4. The evolution of PV for the adiabatic experiment of Fig. 2 at (a) 75°N, (b) 45°N, (c) 15°N, and (d) 45°S. Contour interval is $1.25 \times 10^{-8}$ m$^{-1}$ s$^{-1}$ in (a), $0.75 \times 10^{-8}$ m$^{-1}$ s$^{-1}$ in (b), $0.50 \times 10^{-8}$ m$^{-1}$ s$^{-1}$ in (c), and $0.25 \times 10^{-8}$ m$^{-1}$ s$^{-1}$ in (d). Note the westward propagation at 15°N and 45°S and the eastward propagation (after day 50) at 75°N.

forcing to be introduced without generating strong unbalanced components to the flow. In all the calculations presented here, we have used $\tau = 5$ days, $\varphi_0 = 45°$N, and $\Delta\varphi = 15°$.

The shallow-water equations (1) are numerically integrated, using a global, spectral model at resolution T85. Our code is based on the one developed at NCAR by J. Hack and Collaborators, which we have adapted to incorporate topographic forcing and thermal relaxation; for a detailed discussion of the code, see Browning et al. (1989). To handle the enstrophy cascade to small scales, a standard $\nabla^6$ hyperviscosity is introduced on the right-hand side of (1); we have used a coefficient of $1.0 \times 10^{26}$ m$^6$ s$^{-1}$. The robustness of our numerical results was tested by running several calculations at double the resolution (T170), which permits a smaller hyperviscosity coefficient. The qualitative results are identical at both resolutions; a detailed comparison and discussion of the quantitative impact of resolution on these and similar calculations will be addressed in a forthcoming paper.

## 3. Adiabatic response

In this section we consider the response of a polar vortex to simple topographic forcing in the purely adiabatic case [i.e., we set $\tau_E^{-1} = 0$ in (1)]. The flow is initialized with a zonal wind profile typical of the winter middle stratosphere; it comprises a westerly 50 m s$^{-1}$ jet at 55°N, a zero-wind line around 23°N and

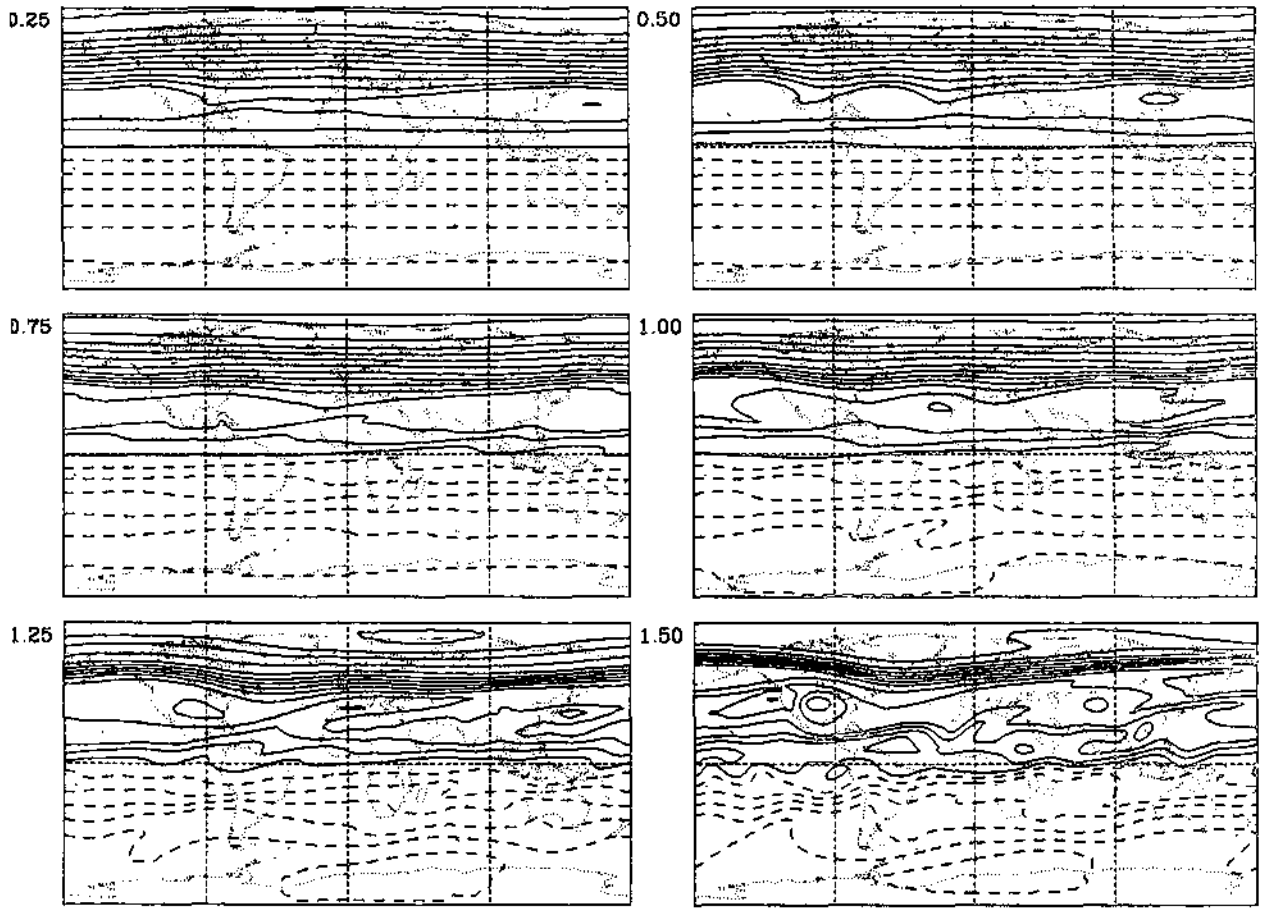


FIG. 5. The PV field at $t = 50$ days for six calculations with parameters identical to the one in Fig. 2, except for the forcing amplitude $H_B$, whose values in km is given next to each frame (the last frame is from Fig. 2). The contour intervals are as in Fig. 2.

weak easterlies at the equator and in the Southern Hemisphere, as shown by the dashed curve in Fig. 1a.

Consider first the response to a forcing of amplitude $H_B = 1500$ m, illustrated in Fig. 2. The effect of the forcing is to produce planetary-scale Rossby wave breaking, which strips air from the edge of the polar vortex, producing steep PV gradients at the edge and a surf zone surrounding the vortex in which the PV is nearly homogenized. Steepening of the PV gradients is manifested in Fig. 2 by the tightening of the contours and can also be seen from the zonal profiles shown in Fig. 1b.

The flow evolution in Fig. 2 shows features typical of nonlinear Rossby wave critical layers (e.g., Haynes 1989) and commonly found in observations of the active winter stratosphere (e.g., Leovy et al. 1985). Specifically, tongues of air are wrapped into midlatitudes from both the polar vortex and the tropics, for example, around 90°W and 90°E on day 20 and around 90°E on day 40. The main surf zone is evident in the zonal average as the region of weak PV gradient (Fig. 1b) between the vortex edge at about 60°N and the northern subtropics. This is where the most intense wave breaking and the consequent large-scale turbulence is located.

Nevertheless, after the initial 30 days or so, weaker wave breaking can be seen to spread into the tropics and proceed all the way to the summer pole. This wave breaking in the summer hemisphere is more clearly seen in Fig. 3, where we have plotted the PV field in polar stereographic projection for day 40 of Fig. 2. The penetration of the wave disturbances, generated by stationary topographic forcing, deep into the easterlies of the summer hemisphere may seem surprising. However, animations of the global PV maps for the calculation shown in Figs. 2 and 3 reveal the presence of a rich spectrum of transient waves. The sequence of events that occurs, illustrated in Fig. 4, is as follows.

In the first 20 days, before the first major wave-breaking event, the quasi-stationary wave increases steadily in amplitude and is confined to middle and high northern latitudes; however, the breaking events generate secondary, transient disturbances that spread rapidly to the southern latitudes. On the vortex edge (cf.

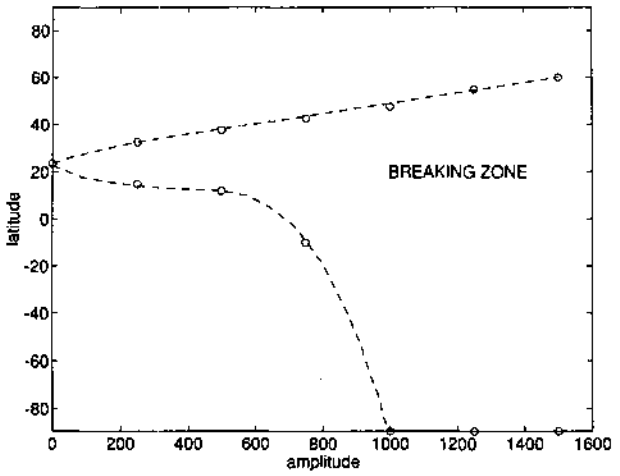


FIG. 6. The width of the breaking region as a function of forcing amplitude $H_B$ for the adiabatic cases of Fig. 5 (see text for details). In the region between the curves (which have been drawn by hand) irreversible deformation of PV contours is found to occur.

Fig. 4a) an eastward propagating disturbance is apparent. [The generation by wave breaking of a similar, apparently normal-mode, transient disturbance on the vortex edge was noted by Polvani and Plumb (1992).] In the tropics (cf. Fig. 4c) westward propagating disturbances dominate and spread far into the summer hemisphere (cf. Fig. 4d); they break throughout this region, though the breaking of these secondary disturbances is weaker than that of the primary wave in the main surf zone. In particular, although there is breaking both ways in the northern subtropics and, on occasion, tropical air is transported into high southern latitudes, no tongues of southern midlatitude air are drawn right across the equator into the main surf zone. Nevertheless, this secondary breaking is sufficiently vigorous and extensive to weaken the effectiveness of the southern edge of the main surf zone as a transport barrier.

We conducted a sequence of experiments to investigate how this behavior depends on the amplitude of wave forcing. In Fig. 5, we show the PV field at $t$ = 50 days for six calculations identical to that shown in Fig. 2 but with a forcing amplitude $H_B$ = 250, 500, 750, 1000, 1250, and 1500 m. It is apparent from the figure that, for $H_B < 750$ m, the wave breaking is confined to a main surf zone in the Northern Hemisphere. However, for this forcing the PV gradient formed at the vortex edge appears much less sharp than is observed in the real wintertime stratosphere. For larger forcing amplitude ($H_B > 750$ m), when stronger PV gradients are formed, wave breaking spreads well beyond the main surf zone.

Thus, for forcing amplitudes able to produce realistic steepening of PV gradients around the vortex, we find in these experiments that the breaking extends well beyond the main surf zone. There are only weak subtropical PV gradients, with breaking across this gradient in both directions (although transport of midlatitude air into the tropics is weaker than that of tropical air into the surf zone; see section 6), and there is extensive breaking in the Southern Hemisphere, which on occasion involves the direct and rapid transport of tropical air into high southern latitudes.

We have quantified the way in which the extent of the breaking region depends on the forcing amplitude. We define the breaking region as that region in which there is sideways overturning in the PV contours; that is, where double-valued contours signify the onset of irreversible contour deformation, the defining property of wave breaking (McIntyre and Palmer 1985; Waugh et al. 1994b). The dependence of width of the breaking region on forcing amplitude is shown in Fig. 6; the latitudes plotted correspond to the zonal mean latitude of the northernmost and southernmost PV contours that overturn. Whereas the latitude of the northern edge of the breaking region (the vortex edge) varies almost linearly with amplitude for all amplitudes in the range we have explored (except perhaps at very small amplitude), the southern edge shows the onset, described above, of breaking outside the main surf zone and the suddenness (as a function of amplitude) with which this breaking extends throughout the summer hemisphere.

## 4. Experiments with thermal relaxation

One key physical ingredient that is missing from the adiabatic dynamics discussed so far is thermal relaxation. The statistically steady state of the established, wintertime vortex is achieved through a balance between, on the one side, erosion by breaking Rossby

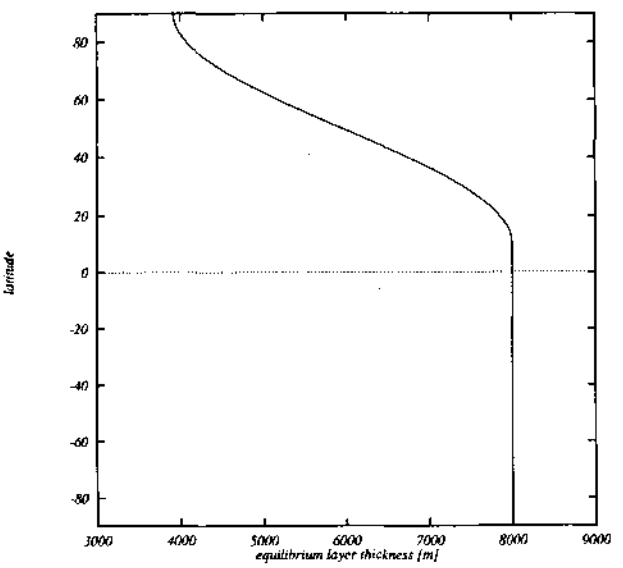


FIG. 7. The equilibrium layer thickness $h_E$ used to model the thermal relaxation process.

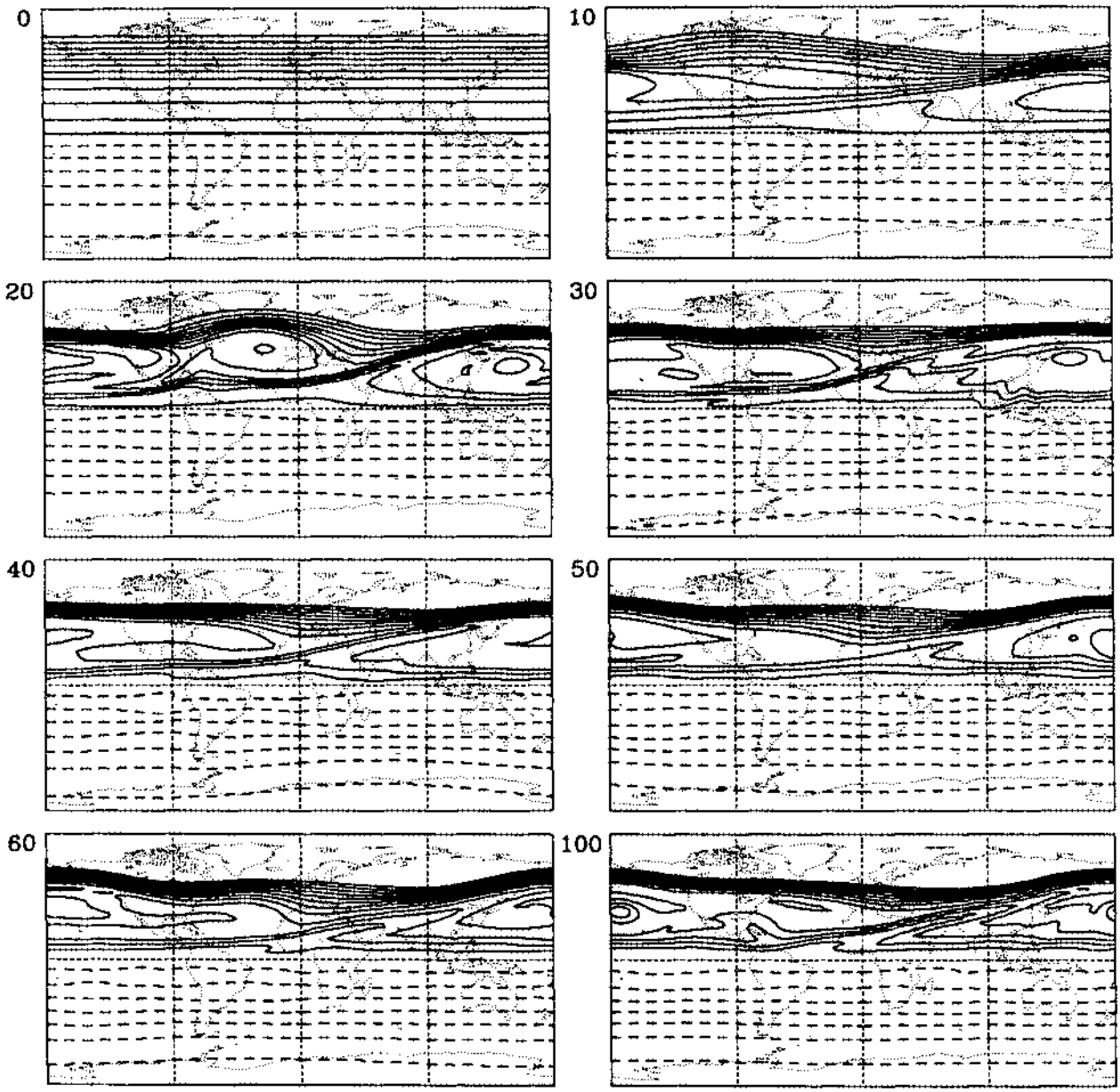


FIG. 8. The response of a polar vortex to topographic forcing in the presence of thermal relaxation; $\tau_E = 10$ days and $h_E$ as given in Fig. 7. See caption to Fig. 2.

waves and, on the other side, regeneration via diabatic adjustment to some radiative equilibrium state (Juckes 1989; Salby et al. 1990b). While nonadiabatic terms have been included in several previous studies, their direct effect on the evolution of the flow has not been clearly assessed. Having independently considered the purely adiabatic response first, we are in a position to show how modification of the subtropical winds by thermal relaxation leads to the formation of steep PV gradients in the subtropics.

We have here opted to choose the term $h_E$ in the last equation of (1) to represent the diabatic effects alone. In other words, we take the term $\tau_E^{-1}(h - h_E)$ to be a crude model of the relaxation of the stratosphere to the *radiative equilibrium temperature*. For this we have chosen a profile for $h_E$ whose shape mimics the latitudinal profile of the Fels–Schwarzkopf radiative equilibrium temperature distribution (see, for instance, Andrews et al. 1987, Fig. 1.2) in the middle stratosphere. In particular, the profile represents the sharp gradient in the middle and high winter latitudes and the flat distribution in the summer hemisphere. However, the profile is modified to eliminate any gradients near the equator, in order to avoid

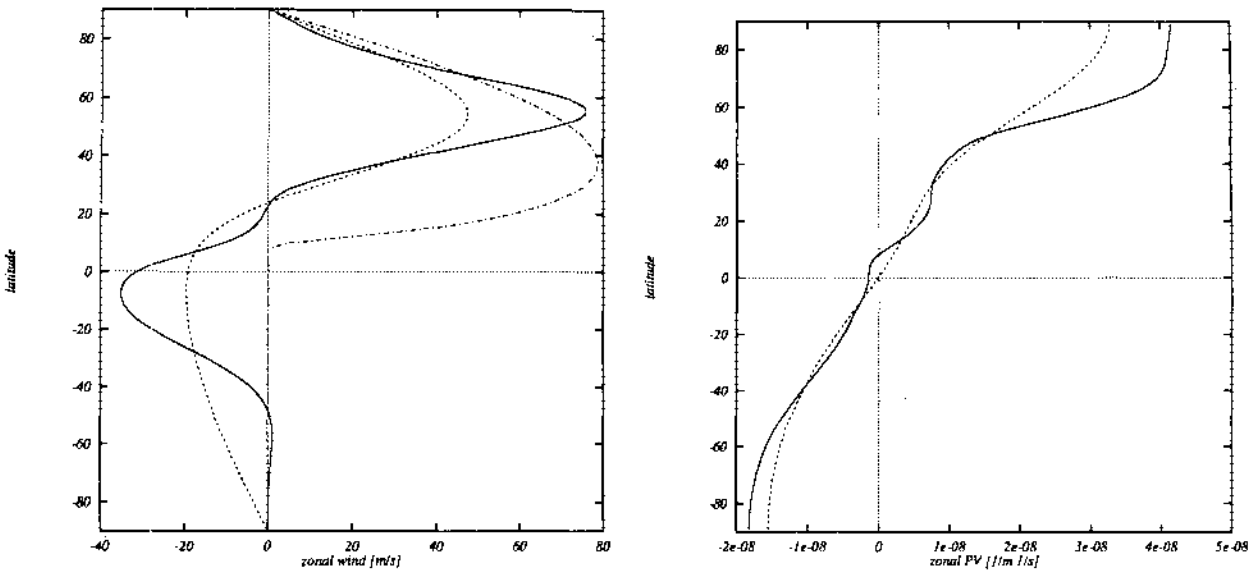


FIG. 9. As in Fig. 1 but for the calculation in Fig. 8. The dashed–dotted line is the zonal wind $u_E$ balanced to the thermal equilibrium profile $h_E$ shown in Fig. 7.

confusing the results by generating a Hadley circulation. (In fact, retaining such gradients proved to have insignificant impact on the results.) The profile $h_E$ used in the calculations presented in this paper is plotted in Fig. 7 (the corresponding balance equilibrium wind $u_E$ is shown in Fig. 9a).

Figure 8 shows the PV from a 100-day integration of the shallow-water equations that has all parameters identical to that shown in Fig. 2, with the exception of the thermal relaxation, for which $\tau_E = 10$ d and $h_E$ as shown in Fig. 7. The contrast between the evolution depicted in Figs. 2 and 8 is quite striking: in the latter, no secondary wave breaking is evident in the Southern Hemisphere and breaking is confined to the main surf zone delimited by two regions of isolated, steep PV gradients. The breaking in Fig. 8 appears to be one-sided at both edges; that is, air is entrained into the surf zone from both polar and tropical regions, without any noticeable reverse transport from the surf zone into the polar vortex or into the tropics. The two edge regions are readily apparent in the tightening of the PV contours in Fig. 8 and are also clearly visible in the zonal PV profile at $t = 100$ d, shown in Fig. 9b, where a subtropical region of steep PV gradients can be seen around 15°N. These regions of steep PV gradients are also clearly visible in the polar stereographic plots of the PV field (shown at $t = 40$ d in Fig. 10a). Notice also the zonality of the Southern Hemisphere in Fig. 10b, compared to the case shown in Fig. 3b.

The temporal evolution of PV, at four different latitudes, for this calculation is shown in Fig. 11; these plots should be contrasted to those in Fig. 4 for the corresponding adiabatic case. The contour levels have been chosen such that Figs. 4 and 11 can be compared directly. It is quite clear that the westward propagating secondary waves are almost entirely suppressed by the presence of the thermal relaxation (Figs. 11c and 11d). It can also be seen from Fig. 11b that the surf zone remains active throughout the calculation, whereas in the adiabatic case (cf. Fig. 4b) the erosion process ceases after the first 50 days or so (see section 6).

The thermal relaxation, moreover, has a very noticeable effect on the poleward edge of the surf zone. Contrasting Figs. 3a and 10a (also, Figs. 2b and 9b), it is quite clear that, paradoxically, *the relaxation* in fact *produces steeper PV gradients* at the *vortex edge*. The vortex is larger in the presence of relaxation, whereas in the purely adiabatic case the vortex has no means of withstanding the erosion and simply retreats to higher latitudes. Contrast the location of the zonally averaged jet maximum (cf. Figs. 1a and 9a); in the adiabatic case it is found near 65°N, whereas with thermal relaxation it is at 55°N.

In order to try to understand more precisely what leads to such a dramatic difference between the adiabatic and nonadiabatic evolutions, we first address the question of whether the relaxation is acting on the waves or mean flow. Inspection of animated PV maps of the case shown in Figs. 9 and 10 reveals that the westward propagating transients noted in the previous section are still present but are weaker and do not break, especially in the summer hemisphere. One possible explanation of this is that these waves are simply dissipated by the thermal relaxation. To test this idea, we replace the term $\tau_E^{-1}(h - h_E)$ with $\tau_E^{-1}(\bar{h} - h_E)$ in (1), where $\bar{h}$ is the zonal average of $h$. With this modification, the evolution in both hemispheres is virtually

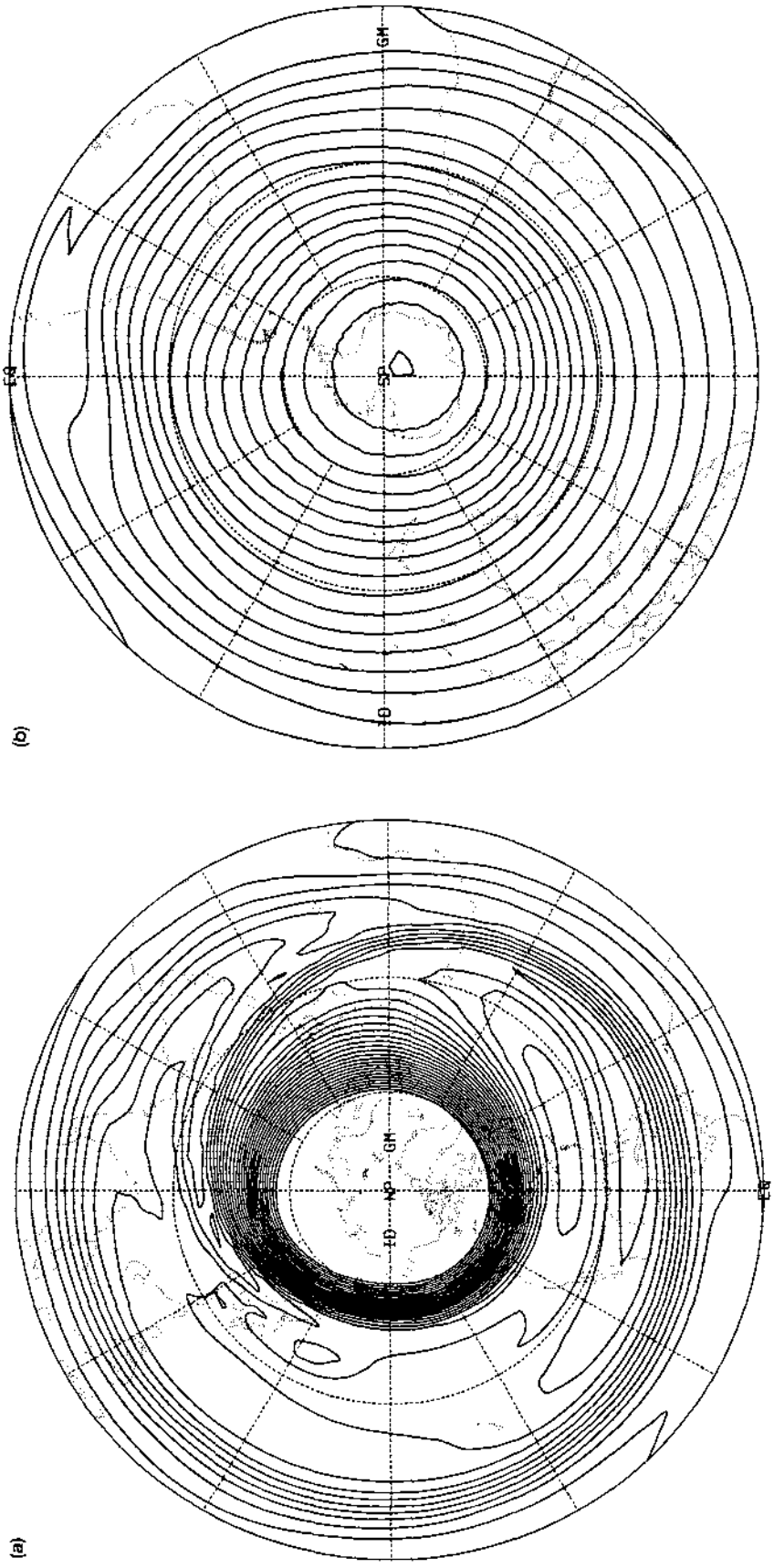


FIG. 10. As in Fig. 3 but for the calculation in Fig. 8.

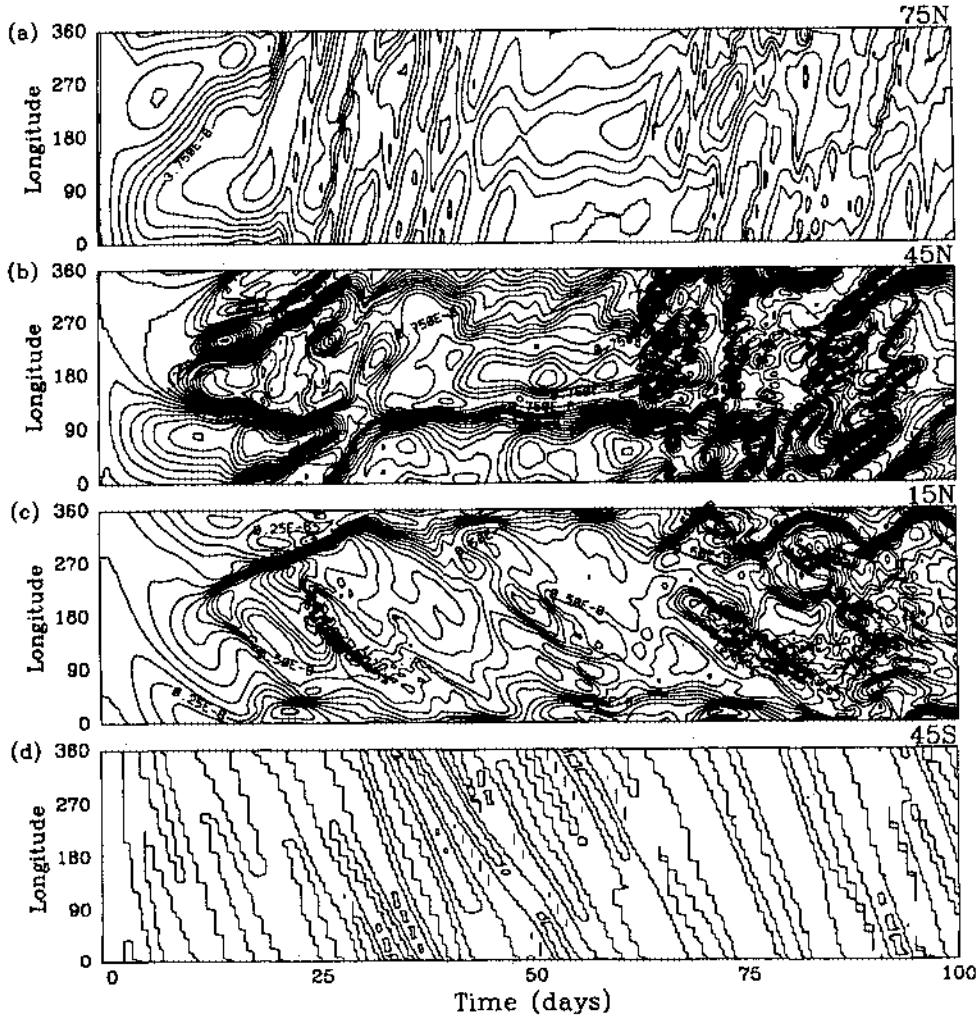


FIG. 11. As in Fig. 4 but for the calculation in Fig. 8. All contour levels are identical to those in Fig. 4.

identical to that of Fig. 8—with a confined surf zone bounded by two regions of steep PV gradients—suggesting that it is the modification of the mean state, rather than of the waves, by the relaxation that prevents the disturbances from propagating to the Southern Hemisphere.

Considering the final states in the calculations with and without thermal relaxation (Figs. 1 and 9), notice that, although the magnitude of the easterlies at the equator is comparable, in the calculation with thermal relaxation there is strong shear in the subtropical region. This suggests that strong shear in the subtropics might be able to confine the breaking region even in the absence of thermal relaxation. To verify this hypothesis, we have examined the adiabatic response in the presence of mean flows with progressively stronger shear in the subtropics. Figure 12 shows three different initial wind profiles: these profiles all have similar shape in the northern midlatitudes (i.e., a virtually identical polar vortex) and progressively larger shear in the subtropics (the solid curve is identical to that in Fig. 1). We have performed three 100-day *adiabatic* integrations starting from each of these three profiles; the PV fields at $t = 60$ d are shown in Fig. 13. For larger tropical shear there is less southward propagation and, thus, elimination of the secondary breaking. We therefore conclude that the confinement of breaking to the main surf zone in these experiments (cf. Fig. 8) is indeed a consequence of the strong subtropical shear induced by the relaxation.

## 5. Ab initio formation of the surf zone

In the experiments described above, as in previously published examples of similar experiments, the flow was initialized with an existing vortex similar to that

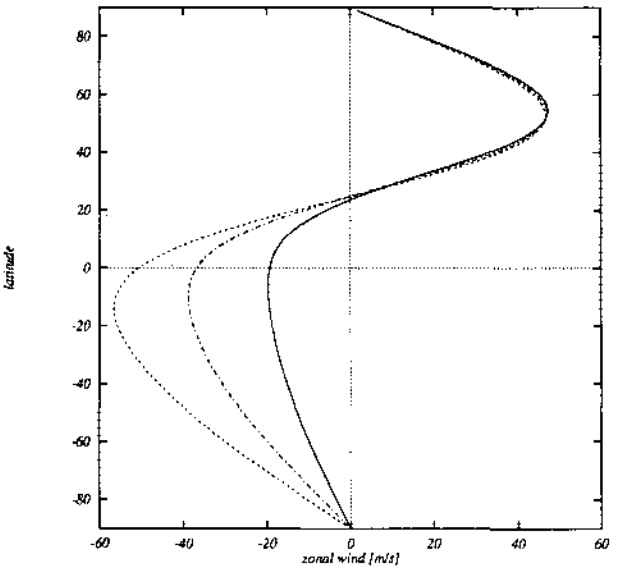


FIG. 12. Three initial zonal wind profiles with increasing shear in the subtropics. The solid line corresponds to the initial profile (dotted line) in Fig. 1.

observed in the winter stratosphere. Here, we show that a simple one-layer shallow-water model is able to capture the vortex formation process. To do this, we start the model with no winds (and thus constant $h$) and let the thermal relaxation and the topographic forcing act on such an initial condition. The choice of $u = 0$ at $t = 0$ seems to be the simplest approximation to flows that are typical of beginning of the early fall. The equilibrium state to which the flow is relaxed is the same as that used above, and is constant in time; we make no attempt to represent seasonal variation of the equilibrium state.

Figure 14 shows the evolution of a calculation with initially zero winds and constant $h$, all other model parameters being identical to the calculation in Fig. 8. It is clearly seen that within a few weeks very steep PV gradients develop in the midlatitudes, marking the formation of a polar vortex. As the vortex forms, steep PV gradients spontaneously develop in the subtropics around 10°N, defining an equatorward edge to the surf zone. The formation of the polar vortex and the subtropical gradients is clearly seen in the mean profiles shown in Fig. 15; it takes around 2 months for the formation of a quasi-steady polar vortex. Note that the jet maximum at $t = 100$ d is found near 53°N (see Fig. 15a), whereas the thermal relaxation would tend to form a jet centered around 34°N (cf. Fig. 9a). The location of jet maximum (i.e., the vortex edge) results from the interplay between the thermal relaxation and Rossby wave breaking (Salby et al. 1990b). As in the previous calculation with thermal relaxation (cf. Fig. 8), air is mixed into the surf zone from the polar vortex and the tropics by means of wave breaking events that draw tongues of air equatorward and poleward, respectively, while the Southern Hemisphere remains relatively quiescent. A careful examination of these tongues and of the mixing process is discussed in the next section.

First, however, we present the results of one more set of calculations. Figure 16 contrasts the zonal profiles at $t = 100$ d from two calculations identical in all respects to the one in Fig. 14, except for the amplitudes of the forcing $h_B$, which are $h_B = 1000$ and 2000 m (in Fig. 14, $h_B = 1500$ m). The evolution in these calculations is qualitatively the same as shown in Fig. 14; however, it is clear, from Figs. 15b and 16, that the main effect of increasing the forcing amplitude is to shift *both* edges of the surf zone poleward. This suggests that a simple explanation for the fact that the region of steep gradients in the subtropics is farther pole-

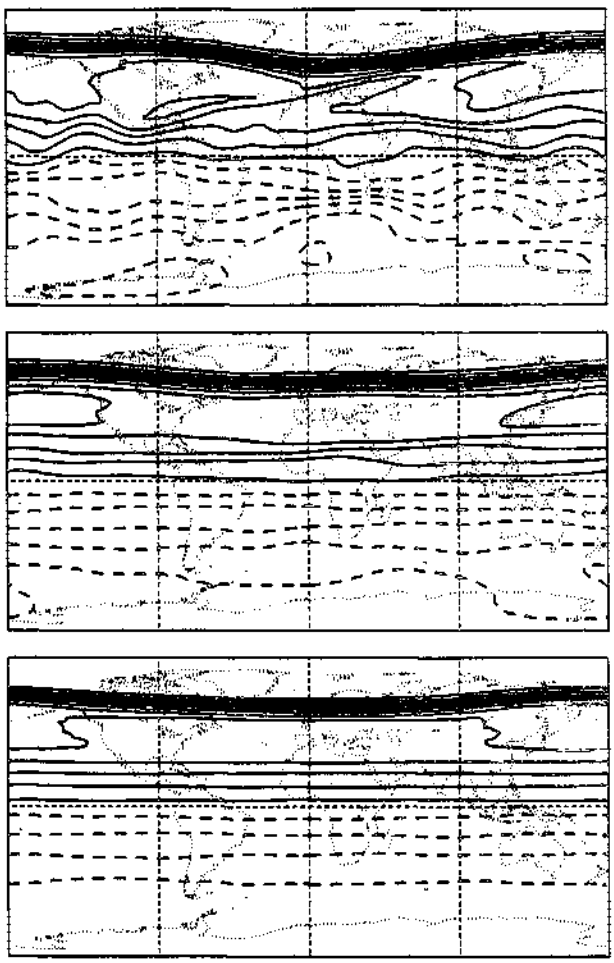

FIG. 13. The PV field at $t = 60$ days for the three profiles of Fig. 12. The {top, middle, bottom} figures correspond to the {solid, dashed–dotted, dotted} initial profiles in Fig. 12; that is, subtropical shear is smallest for the top figure and largest for the bottom one. Note how the stronger subtropical shear confines the surf zone to a narrow latitudinal band. Contour levels are as in Fig. 1.

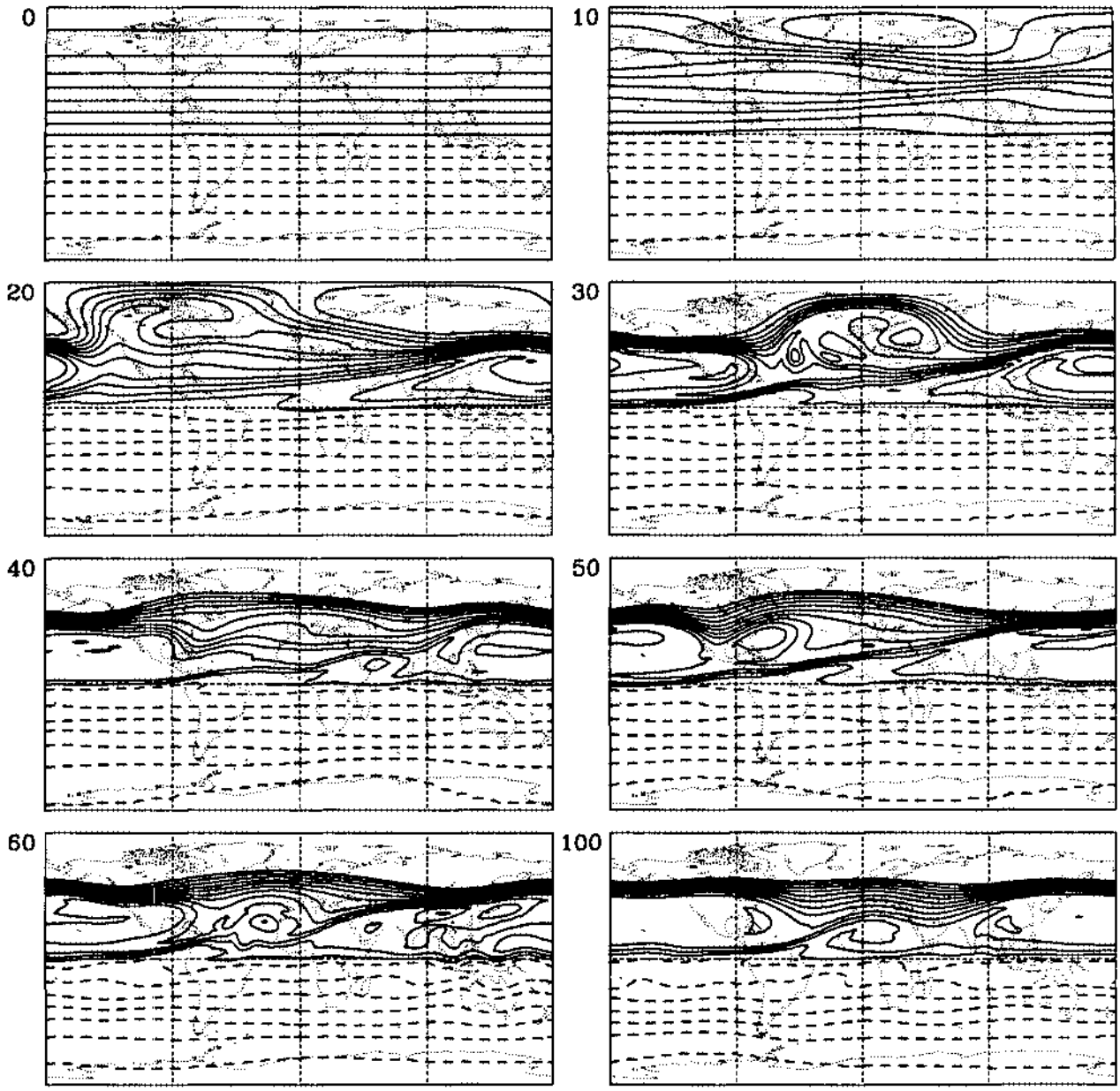


FIG. 14. The PV field showing the formation of a polar vortex and a latitudinally confined surf zone, starting from a state of rest. Contour levels are as in Fig. 2.

ward in the northern winter than in the southern winter (Randel et al. 1993) may simply come from the fact that the forcing is greater in the former case, as is well known from the fact that the northern winter vortex is smaller and much more perturbed than its southern counterpart.

## 6. Transport into the surf zone

In this section we examine in more detail the tracer transport in the calculations presented in the previous sections. In particular, we quantify the transport into the midlatitude surf zone from both the polar vortex and the tropics. To enable an examination of the fine-scale tracer transport, we perform calculations using the contour advection (CA) technique (Waugh and Plumb 1994; Norton 1994); this technique allows examination of the evolution of material contours in a specified evolving flow at scales much smaller than those of a specified flow. [Bowman (1993), Pierce et al. (1993), and Pierce and Fairlie (1993) have also used trajectory calculations to examine transport in numerical simu-

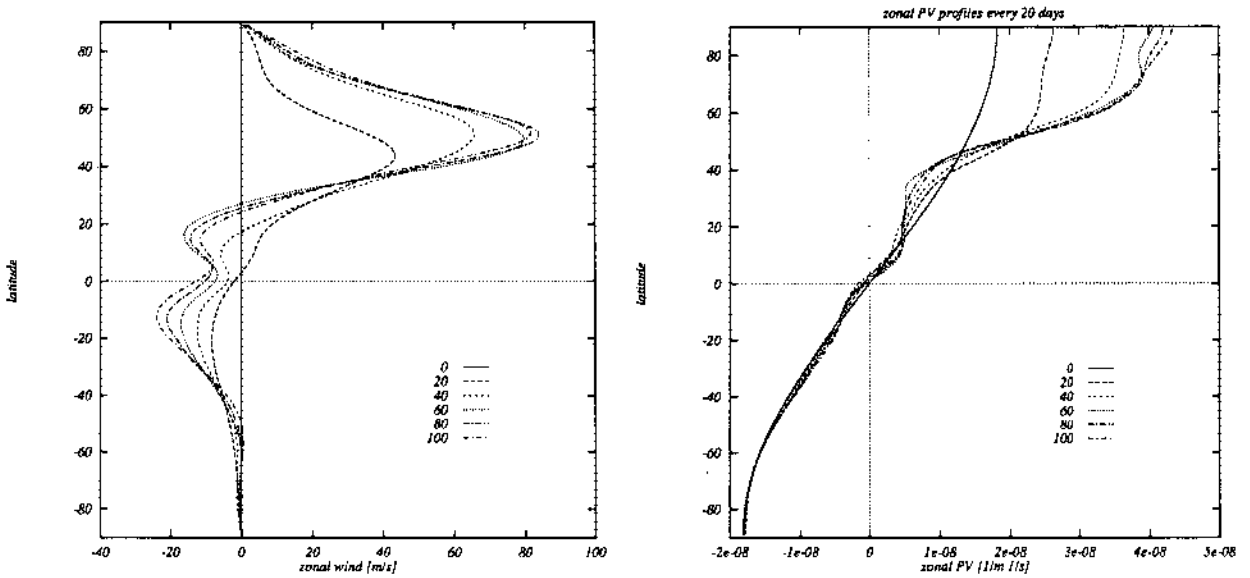


FIG. 15. Zonally averaged (a) wind and (b) potential vorticity profiles for the calculation in Fig. 14. To show the evolution of the flow, profiles are plotted at $t$ = 0, 20, 40, 60, 80, and 100 days.

lations.] Full details of the CA technique, including demonstrations of its accuracy, are given in Waugh and Plumb (1994); comparisons of results from CA calculations with in situ aircraft observations of chemical tracers are shown in Plumb et al. (1994) and Waugh et al. (1994a).

The maps of PV shown in previous sections show Rossby wave breaking events with tongues of air being drawn into the surf zone from both the polar vortex and the tropics (e.g., Figs. 2, 8, and 14). The structure of these wave breaking events can be seen more clearly in CA calculations. For example, Fig. 17 shows the results of a CA calculation using the winds from the calculation shown in Fig. 8. The CA calculation was initialized with the PV = $0.25 \times 10^{-8}$ and $1.125 \times 10^{-8}$ m$^{-1}$ s$^{-1}$ contours at day 10; these two contours were chosen because they are representative of the tropical and polar edges, respectively, of the surf zone. This

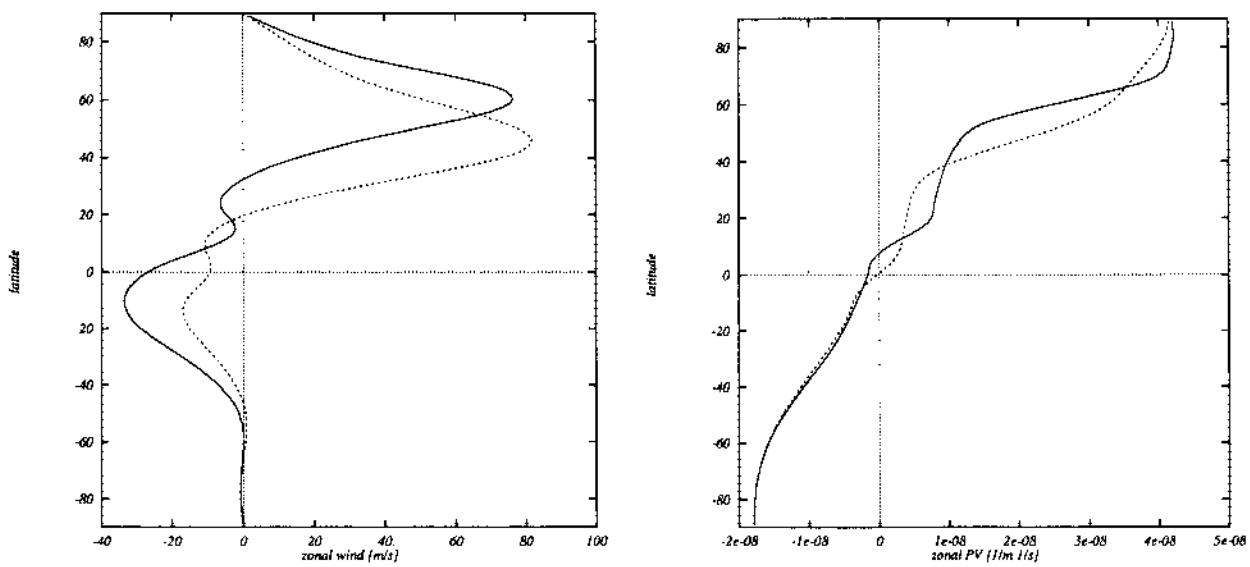


FIG. 16. Zonally averaged (a) wind and (b) potential vorticity profiles at $t$ = 100 days for experiments identical to the one in Fig. 14 except with different forcing amplitudes: $H_B$ = 1000 m (dashed line) and $H_B$ = 2000 m (solid line). Note how increasing the amplitude shifts the regions of steep PV gradients poleward.

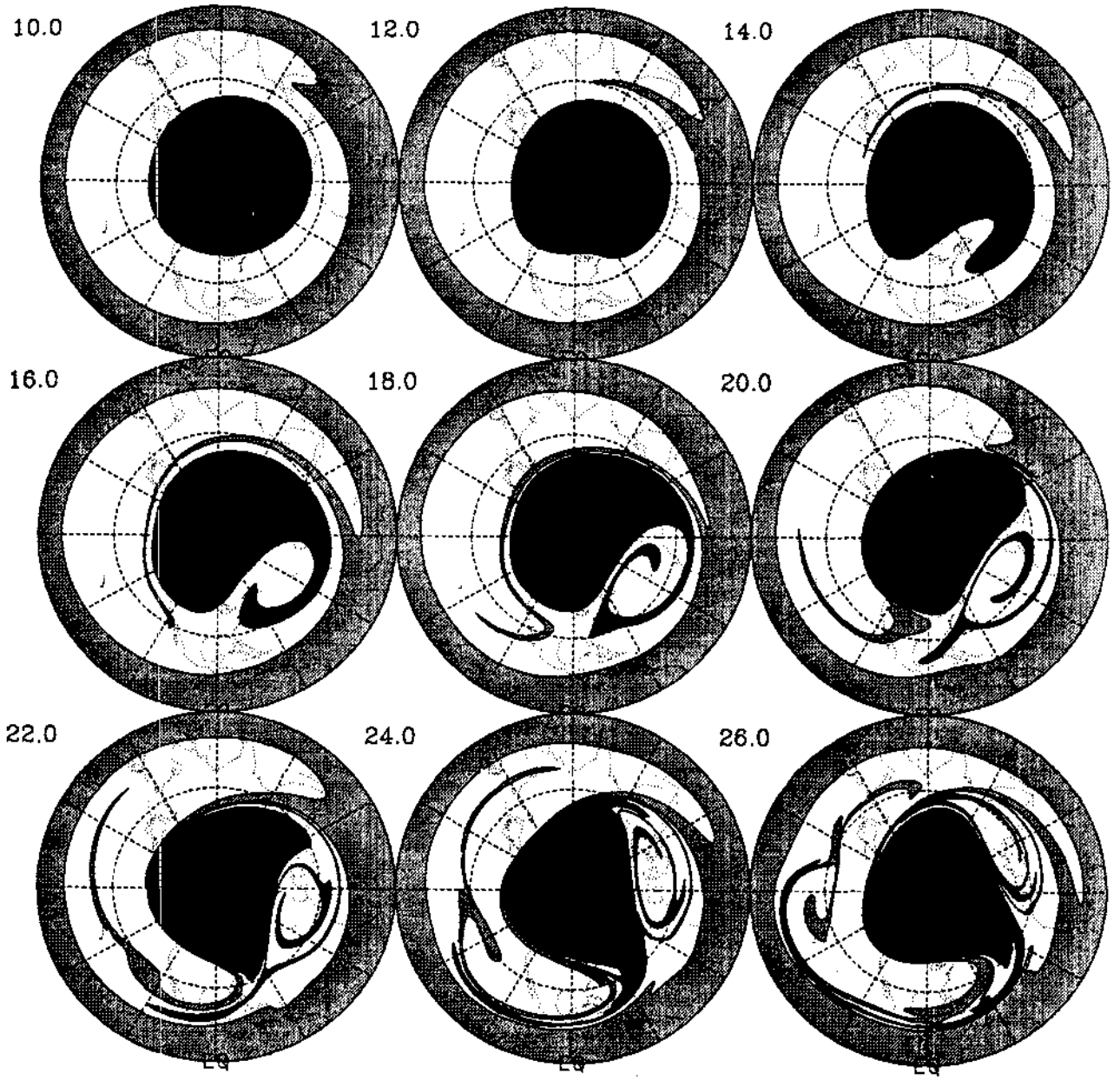


FIG. 17. Results from a CA calculation using the winds from the shallow-water calculation shown in Fig. 8. The calculation was initialized with the PV = $0.25 \times 10^{-8}$ and $1.125 \times 10^{-8}$ m$^{-1}$ s$^{-1}$ contours at day 10. Time, in days, is in the upper left-hand corner of each plot. Maps are polar stereographic projections, with the Greenwich meridian to the right.

calculation shows fine-scale tongues of both subtropical and vortex air that are absent from the PV maps. During the period shown in Fig. 17, the edge of the disturbed polar vortex extends toward low latitudes and draws tongues of tropical air into middle latitudes (e.g., at 45°E on days 10–12 and 20–22). These tongues of tropical air are stretched and wrapped around the edge of the vortex. Simultaneously, a tongue of polar air is extruded from the vortex edge (e.g., at 30°W on day 14) and entrained into the surf zone. Note that, as mentioned in section 4, there is no transport from the surf zone into either the polar vortex or the Tropics.

Breaking events similar to that shown in Fig. 17 occur throughout the shallow-water calculation shown in Fig. 8; Fig. 18 shows the results of four 10-day CA calculations initialized at different times during the calculation. The evolution during all events is qualitatively the same: tongues of both polar vortex and tropical air

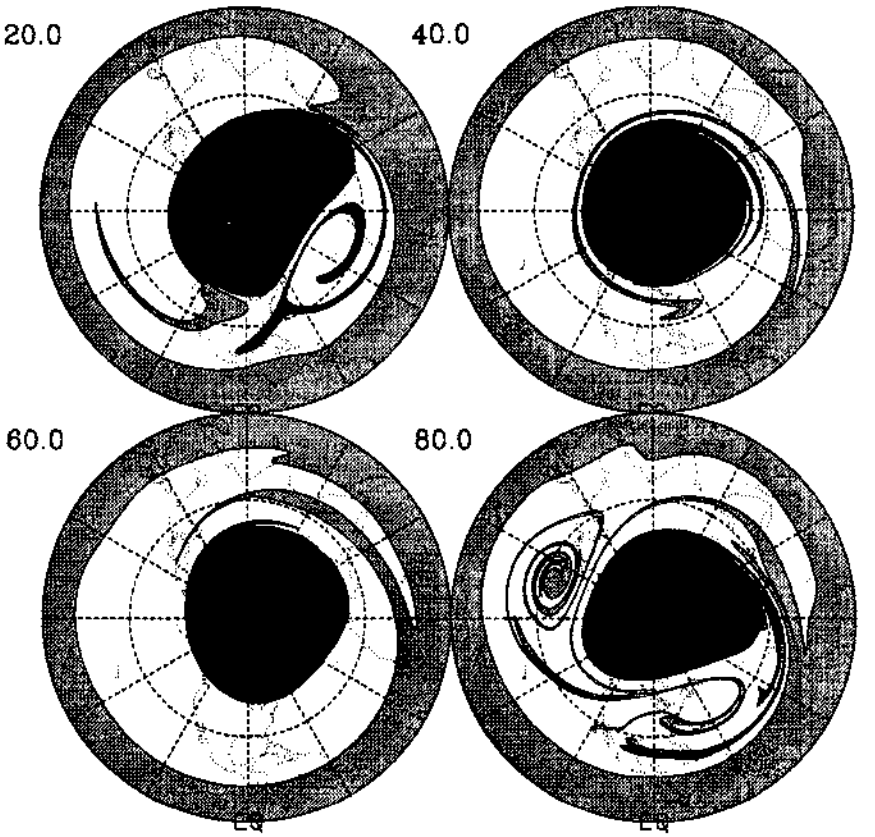


FIG. 18. Results from four 10-day CA calculations, using the winds from the shallow-water calculation shown in Fig. 8, initialized at day (a) 10, (b) 30, (c) 50, and (d) 70. Each calculation was initialized with the PV = $0.25 \times 10^{-8}$ and $1.125 \times 10^{-8}$ $m^{-1}$ $s^{-1}$ contours. Map projection is the same as in Fig. 17.

are transported into the surf zone and wrapped around the polar vortex, and there is no transport into the polar vortex or Tropics. There is, however, variability in the amount of air transported into the surf zone; this is quantified below.

In the calculations with no thermal relaxation (e.g., Fig. 2), tropical and polar vortex air is transported into the surf zone in the same manner described above. Figure 19 shows the results of CA calculations initialized at different times during the calculation shown in Fig. 2. At early times the distribution is very similar to that in the calculations with thermal relaxation: thin tongues of polar vortex and tropical air are wrapped into the surf zone. At later times, however, the distribution is different from that in the calculations with thermal relaxation: the vortex is considerably smaller (because of vortex erosion; see section 4), and there is only weak wave breaking with very little transport into the surf zone.

The calculations in Fig. 19 also show that, in the absence of thermal relaxation, there is also some transport from the surf zone into the Tropics (but there is still no transport into the vortex). For example, at 135°E and 120°W on day 40 there is a thin tongue of midlatitude air intruding into the tropical region. In section 4 it was shown that strength of the tropical shear was an important factor in determining the confinement of the breaking within the surf zone. One can assess the affect of the tropical shear on the transport into and out of the tropics by comparing CA calculations using winds from the three adiabatic calculations, with different tropical shear, shown in Fig. 13. Figure 20 shows the results of three 10-day CA calculations for each of the calculations in Fig. 13. With increasing shear (Fig. 13a–c) there is more transport out of the tropics and less transport into the tropics (in all cases the transport into the tropics is much weaker than that out of the tropics); hence, steeper subtropical gradients form with increasing tropical easterly shear.

One may estimate the amount of air transported into the surf zone during the above breaking events by defining the boundaries of the various regions. Previous studies have used various criteria for defining the edge of the polar vortex and, hence, the polar edge of the surf zone (e.g., a critical value of PV, maximum PV gradient, or maximum wind speed). However, as dis-

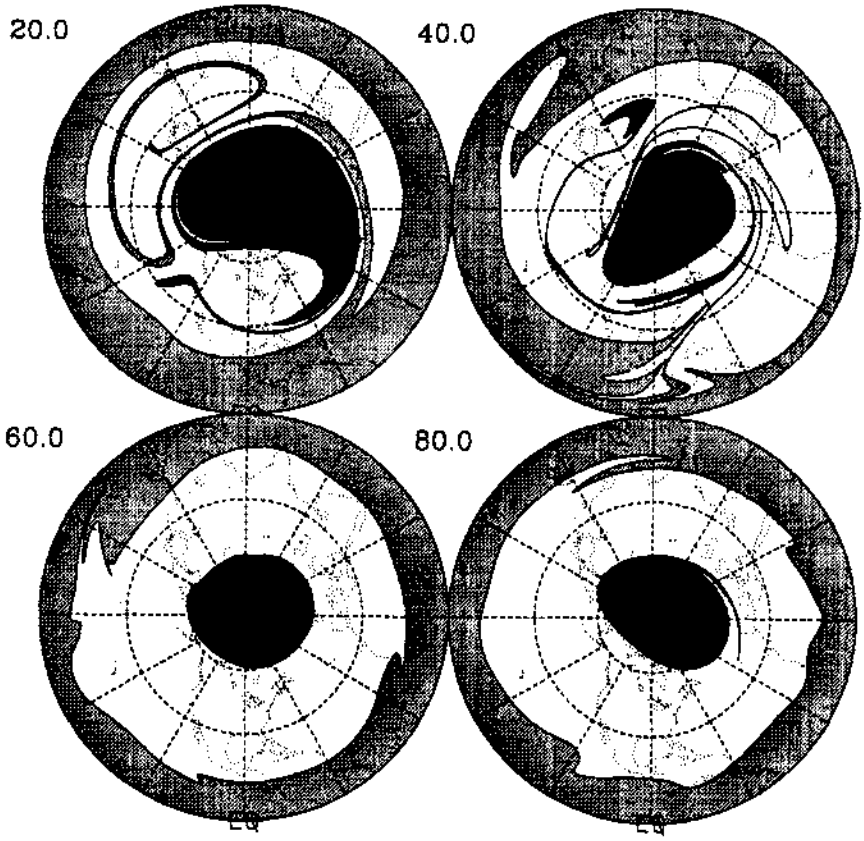


FIG. 19. As in Fig. 18, except with winds from the shallow-water calculation shown in Fig. 2, and initial contours were the PV = $0.375 \times 10^{-8}$ and $1.375 \times 10^{-8}$ $m^{-1}$ $s^{-1}$ contours. With reference to Fig. 18, notice how the absence of thermal relaxation leads to greater erosion of the vortex, the eventual arrest of Rossby wave breaking, and the decay of the associated transport (cf. Fig. 23).

cussed in Waugh et al. (1994a,b), it is difficult to uniquely define the edge of the polar vortex; the same difficulties also exist for defining the tropical edge of the surf zone. The calculated transport into the surf zone will depend greatly on the definition used to calculate the surf zone boundaries.

With this in mind, we have chosen here to use the "coarse-graining" procedure of Waugh (1992) (see also Dritschel and Waugh 1992 and Waugh et al. 1994a) to calculate the boundaries. In this coarse-graining procedure, the surgical part of the contour surgery algorithm (Dritschel 1989) is applied repeatedly, iteratively increasing the surgical cutoff scale $\delta$ up to a value of 0.05 times the earth's radius ($\delta \approx 300$ km). This procedure automatically and efficiently removes filamentary structures and isolates the large-scale boundaries of the surf zone. For instance, Fig. 21 compares the contours at day 20 in the CA calculation shown in Fig. 17 with the coarse-grained contours that are used as the boundaries of the surf zone.

As a simple estimate of transport into the surf zone, we calculate the area of polar and tropical air that is entrained. Note that the change in depth in the shallow-water calculations is small, and the variation in the area enclosed by contours is very similar to the variation of the volume. The area of air transported across the surf zone boundaries is determined by calculating the difference in area between the original contour and the coarse-grained contour, that is, the difference in area between the shaded regions and solid contours in Fig. 21.

Table 1 contains the estimated transport between days 10 and 20 of the calculation shown in Fig. 8 (see also Fig. 17) for different choices of the surf zone boundaries; $A_p$ is the area enclosed by the polar boundary of the surf zone, $A_t$ the area enclosed by the tropical boundary, and $A_{ex\text{-}p}$ and $A_{ex\text{-}t}$ the area of air transported into the surf zone from the polar vortex and the tropics, respectively. These calculations show the aforementioned sensitivity to the definition of the surf zone boundary. As the surf zone boundaries are moved toward the center of the surf zone (e.g., reading down Table 1), the amount of transport into the surf zone increases. The wave breaking "strips" air mainly from

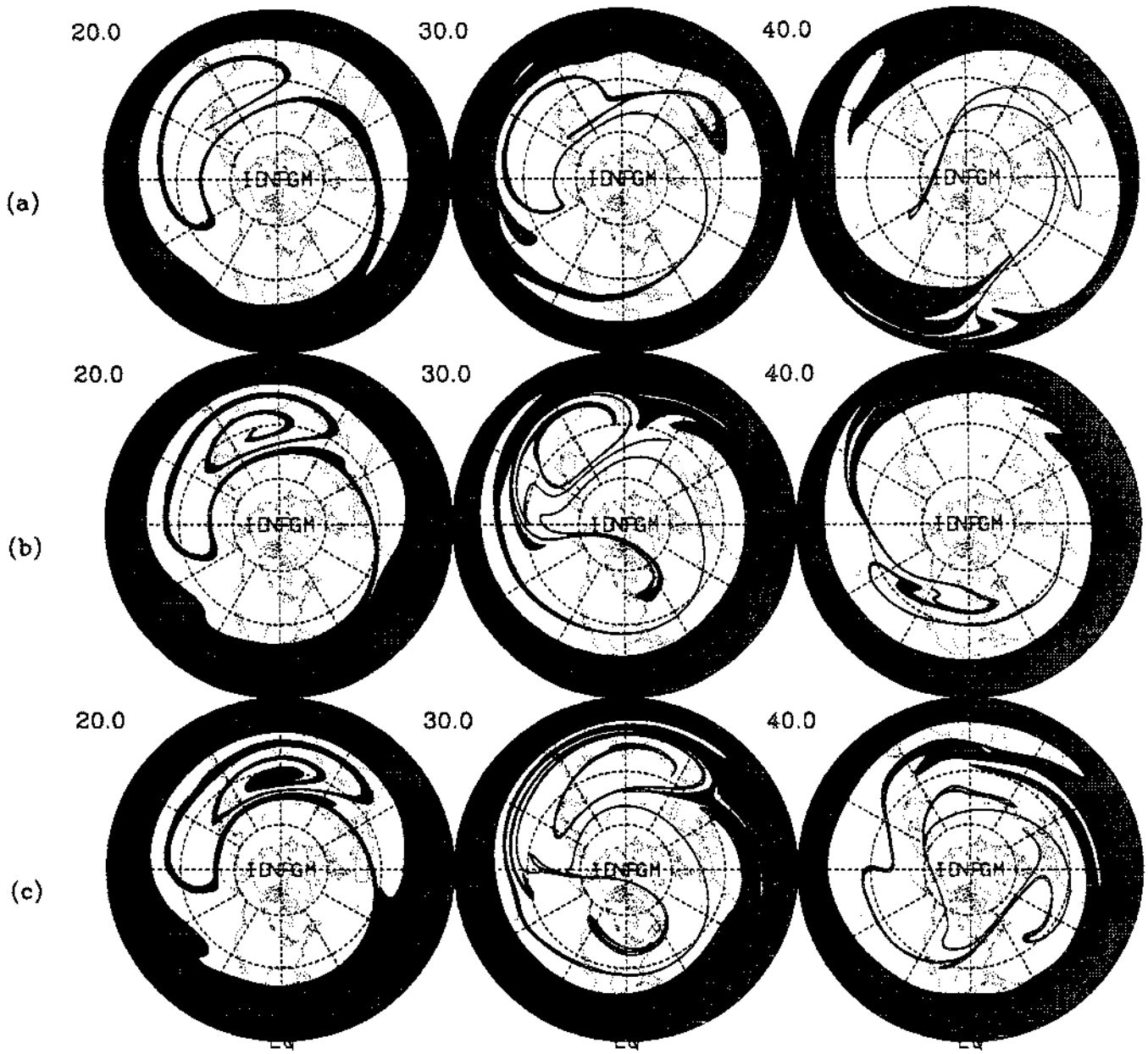


FIG. 20. Results from 10-day CA calculations initialized at days 10, 20, and 30, using the winds from the shallow-water calculations shown in Fig. 13a–c. The initial conditions in the calculations (a) to (c) have increasing initial tropical shear. Each calculation was initialized with the PV = $0.375 \times 10^{-8}$ m$^{-1}$ s$^{-1}$.

the outer edges of both the polar vortex and the Tropics, and there is negligible transport from well inside these regions.

The temporal variation of the transport into the surf zone for the shallow-water calculations shown in Figs. 8 and 2 (see also Figs. 18 and 19) is shown in Figs. 22 and 23, respectively. These figures show the estimated transport within 10 days for periods covering the duration of the two shallow-water calculations. The amount of air transported into the surf zone from both the polar vortex and the Tropics varies between different time periods and the different calculations; in general, for periods when there is decreased transport from the polar vortex there is also decreased transport from the Tropics.

Also shown in Figs. 22 and 23 is the temporal variation of the minimum latitude of the vortex edge (as defined by PV contours). Comparing this with the transport rates, we see that, as has been noted previously (e.g., Leovy et al. 1985; Waugh 1993b), there is

a strong relationship between the transport into the surf zone and the movement of the vortex edge; when the edge of the vortex reaches low latitudes, there is large transport out of the Tropics. Note that in the latter half of the adiabatic calculation the vortex edge never reaches low latitudes (because of erosion by wave breaking) and hence there is very little associated transport.

In the calculation with thermal relaxation, the average area transported into the surf zone, per 10 days, from the polar vortex and the tropics is 1.2% and 3.5%, respectively, of the surf zone area; this corresponds to 11% and 32%, respectively, over a 3-month period. The transport rates into the surf zone during the first half of calculation without thermal relaxation are similar to those in the calculation with thermal relaxation, but, as noted above, there is negligible transport during the latter half. It is important, however, to emphasize that the amounts of transport thus determined are very sensitive to the definition of surf zone boundaries.

TABLE 1. Estimated transport into the surf zone during days 10 to 20 for different definitions of surf zone boundary, obtained from CAS calculations using winds from the experiment shown in Fig. 8. $PV_{edge}$ is the potential vorticity (in units $10^{-5}$ m$^{-1}$ s$^{-1}$) used in forming the coarse-grain boundaries of the surf zone. $A_p$ is the area enclosed by the polar boundary of the surf zone, $A_t$ the area enclosed by the tropical boundary, and $A_{ex-p}$ and $A_{ex-t}$ the area of air transported into the surf zone from the polar vortex and the tropics, respectively. Areas are expressed as a percentage of the area of a hemisphere.

| $PV_{edge}$ | $A_p$ | $A_{ex-p}$ | $PV_{edge}$ | $A_t$ | $A_{ex-t}$ |
|---|---|---|---|---|---|
| 1.750 | 20.6 | 0.4 | 0.000 | 94.5 | 0.0 |
| 1.500 | 24.2 | 0.5 | 0.125 | 85.8 | 0.3 |
| 1.250 | 28.2 | 1.0 | 0.250 | 78.1 | 2.7 |
| 1.125 | 29.9 | 2.2 | 0.375 | 53.5 | 6.8 |

## 7. Discussion

In all the experiments described here, we have found meridional transport to maximize in the main surf zone of the winter hemisphere, lying between a well-defined polar vortex and the tropics. Within this region, tongues of both vortex and tropical air are intermittently entrained in the flanks of surf zone anticyclones and stretched into long, thin filaments before being mixed down further into more convoluted structures distributed throughout the surf zone. The stretching is especially rapid in the strong shear on the equatorward side

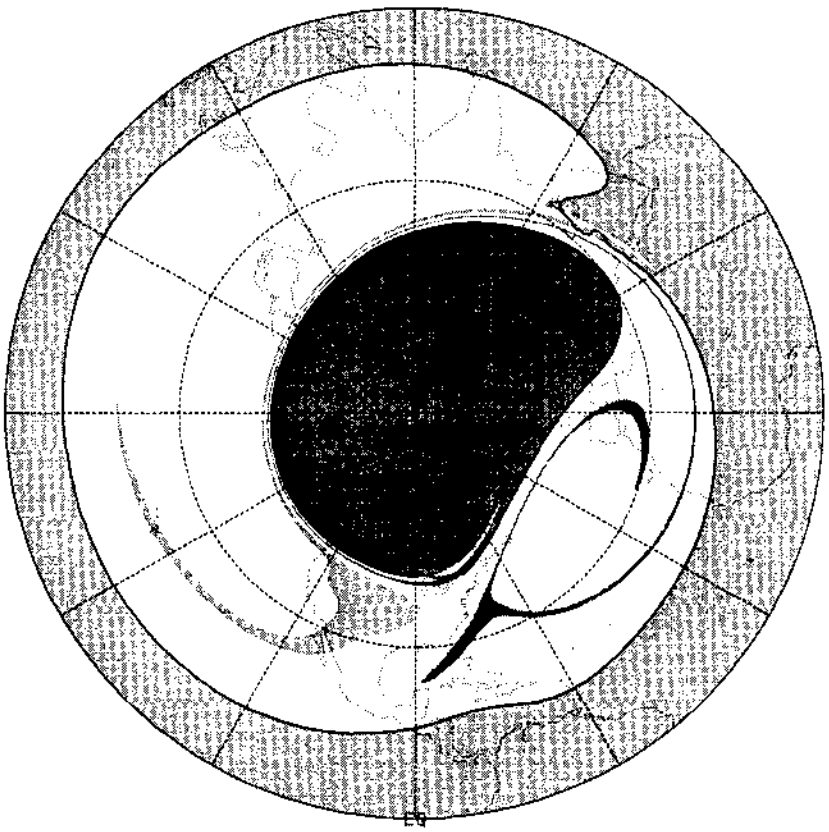

FIG. 21. Comparison of contours at day 20 in the CA calculation shown in Fig. 17 (shaded regions) with the coarse-grained contours (solid curves) that are used as the boundaries of the surf zone. Map projection is the same as in Fig. 17.

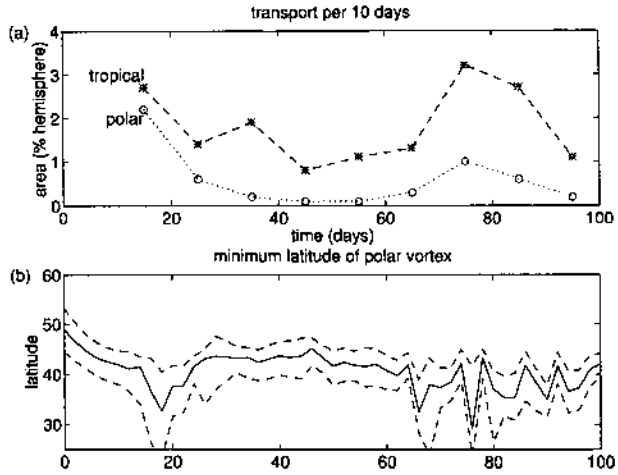


FIG. 22. (a) The estimated transport, within 10 days, into surf zone from tropics (crosses and dashed line) and from polar vortex (circles and dotted line) in shallow-water calculation shown in Fig. 8. See text for details. (b) Minimum latitude of three PV contours at edge of vortex in calculation shown in Fig. 8; lower, middle, and upper contours are for PV = (1.25, 1.5, 1.75) $\times 10^{-8}$ m$^{-1}$ s$^{-1}$, respectively.

of the polar jet, just outside the vortex edge, and in most cases and at most times the CA results show filaments of both polar and tropical air strung around the vortex edge, thus making this a preferred region for the interaction of these two different air masses. For reasons already noted, it is difficult to quantify with any precision the net transport rates into the surf zone; on the basis of the calculations described in section 6, however, we estimate that there is rather more tropical air than polar air entrained into the surf zone.

Despite this overall common behavior, a key result of this paper is that the confinement of wave breaking to the main surf zone and, correspondingly, the sharpness and impermeability of its subtropical edge, falls into one of two regimes: an "unconfined breaking" regime and a "confined breaking" regime. In the unconfined breaking regime, the wave breaking extends beyond the main surf zone all the way to high summer latitudes; moreover, breaking at the subtropical edge comprises both entrainment into the surf zone and, somewhat more weakly, intrusion of midlatitude air into the tropics. In contrast, in the confined breaking regime the breaking is confined to the winter hemisphere surf zone, and the subtropical edge of the surf zone is both sharp and impermeable to equatorward intrusion of midlatitude air; then in this regime, air is entrained into the surf zone from both directions, without detrainment into either the polar vortex or the tropics.

The calculations performed in this study seem to follow the following pattern. In the absence of thermal relaxation the evolution of the flow was found to lie in the confined breaking regime only when the topographic Rossby-wave forcing is weak. At larger amplitudes (i.e., such that the size of the polar vortex, the sharpness of the PV gradients, and the extent of the main surf zone appear to resemble those of the observed winter stratosphere) the evolution is in the unconfined breaking regime. In contrast, in the calculations performed with a thermal relaxation the flow is always in the confined breaking regime.

The mechanism by which Rossby wave activity propagates into the summer hemisphere and leads to extensive wave breaking is a subtle one. Major events in which the forced stationary wave breaks generate secondary Rossby waves that propagate eastward along the westerly jet at the vortex edge and westward at the tropical edge of the surf zone. In the adiabatic series of experiments described in section 2, these westward propagating waves are able to penetrate the easterly tropical winds and spread throughout the summer hemisphere. At sufficiently large wave amplitudes, the waves break throughout this region, effecting transport into the tropics from the surf zone and throughout the summer hemisphere. It was found that the penetration of these transient waves into and through the tropics was inhibited in experiments with strong easterly shear in the winter subtropics (more specifically, with greater easterly wind difference between midlatitudes and tropics). This occurred naturally in those experiments with thermal relaxation.

The importance of the tropical shear in determining the confinement of the wave breaking suggests that the results in this paper may be of some relevance in understanding the effect of the phase of the QBO on transport in the extratropics. In the easterly phase of the QBO there is greater easterly shear and, from the above results, one would expect the subtropical gradients to be steeper than in the westerly phase, consistent with the observations of tropical aerosols (Trepte and Hitch-

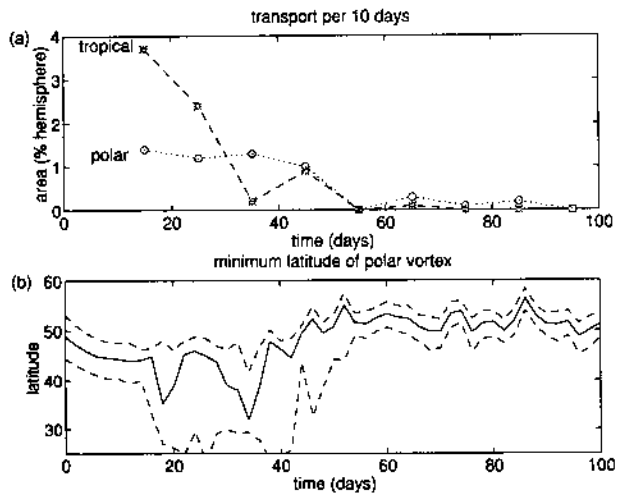


FIG. 23. As in Fig. 22 except for the adiabatic calculation shown in Fig. 2.

man 1992). Note, however, that the presence of steeper gradients in the easterly phase does not necessarily imply weaker transport out of the subtropics (see, for instance, Fig. 20); the steeper gradients may in fact be *a consequence* of the stronger transport.

We are inevitably led to ask which of the above two regimes is closer to the situation in the winter stratosphere. It is difficult to make any theoretical predictions on the basis of these results, as the differences in zonal wind between tropics and winter midlatitudes—in both calculated radiative equilibrium and observed states—vary strongly with height through the stratosphere and, given the apparently deep nature of stratospheric wave dynamics, these single-layer results are unlikely to be applicable layer by layer.

It is not clear that the observational evidence for tropical isolation (noted in the introduction) precludes weak wave breaking into the tropics. Interpretation of results from CA using winds from stratospheric analyses (such as in Waugh 1993b) is so clouded by the uncertainties in the tropical winds that no robust conclusion can be reached. Inspection of the evolution of potential vorticity in the summer stratosphere, calculated from stratospheric analyses, sometimes reveals hints of weak wave breaking but it is not clear whether this is really occurring, nor, if it is, whether it is induced by secondary Rossby waves from the winter hemisphere. All in all, we cannot determine from current observational data which of the two regimes better represents atmospheric behavior. Preliminary investigations we have made using output from the high-resolution GFDL "SKYHI" general circulation model (Mahlman and Umscheid 1987) indicate that the flow in that model is closer to the confined breaking regime. However, further analysis—involving both sophisticated models and stratospheric data—will be required to resolve the issue.

*Acknowledgments.* We are grateful to M. McIntyre and D. O'Sullivan for suggesting improvements on the original version of this paper; to J. Hack, J. Browning, and R. Jacob for useful discussions on the numerical details of the spectral code; and to W. Norton for many friendly interactions of this subject. The computations presented here were performed on the Cray-YMP at the Pittsburgh SuperComputing Center. This work was supported by the National Science Foundation under Grant ATM-92-17844 to Columbia University and Grant ATM-92-18841 to MIT.

## REFERENCES

Andrews, D. G., H. R. Holton, and C. B. Leovy, 1987: *Middle Atmosphere Dynamics.* Academic Press, 489 pp.

Boville, B. A., J. R. Holton, and P. W. Mote, 1991: Simulation of the Pinatubo aerosol cloud in general circulation model. *Geophys. Res. Lett.,* **18,** 2281–2284.

Bowman, K. P., 1993: Barotropic simulation of large-scale mixing in the Antarctic polar vortex. *J. Atmos. Sci.,* **50,** 2901–2914.

Browning, G. L., J. J. Hack, and P. N. Swarztrauber, 1989: A comparison of three numerical methods for solving the shallow water equations on the sphere. *Mon. Wea. Rev.,* **117,** 1058–1075.

Dritschel, D. G., 1989: Contour dynamics and contour surgery: Numerical algorithms for extended, high-resolution modeling of vortex dynamics in two-dimensional, inviscid, incompressible flows. *Comput. Phys. Rep.,* **10,** 77–146.

——, and D. W. Waugh, 1992: Quantification of inelastic interactions of vortices in two-dimensional vortex dynamics. *Phys. Fluids A,* **4,** 1737–1744.

Dyer, A., and B. B. Hicks, 1968: Global spread of volcanic dust from the Bali eruption of 1963. *Quart. J. Roy. Meteor. Soc.,* **94,** 545–554.

Feely, H. W., and J. Spar, 1960: Tungsten-185 from nuclear bomb tests as a tracer for stratospheric meteorology. *Nature,* **188,** 1062–1064.

Grant, B. G., and Coauthors, 1994: Aerosol associated changes in the tropical stratospheric ozone following the eruption of Mount Pinatubo. *J. Geophys. Res.,* **99**(4), 8197–8211.

Haynes, P. H., 1989: The effect of barotropic instability on the nonlinear evolution of a Rossby wave critical layer. *J. Fluid Mech.,* **207,** 231–266.

Hoskins, B. J., M. E. McIntyre, and A. W. Robertson, 1985: On the use and significance of isentropic potential-vorticity maps. *Quart. J. Roy. Meteor. Soc.,* **111,** 877–946; see also **113,** 402–404.

Juckes, M. N., 1989: A shallow water model of the winter stratosphere. *J. Atmos. Sci.,* **46,** 2934–2955.

——, and M. E. McIntyre, 1987: A high resolution, one-layer model of breaking planetary waves in the winter stratosphere. *Nature,* **328,** 590–596.

Leovy, C. B., C. R. Sun, M. H. Hitchman, E. E. Remsberg, J. M. Russell, L. L. Gordley, J. C. Gille, and L. V. Lyjak, 1985: Transport of ozone in the middle atmosphere: Evidence for planetary wave breaking. *J. Atmos. Sci.,* **42,** 230–244.

Mahlman, J. D., 1985: Mechanistic interpretation of stratospheric tracer transport. *A. Climate Dynamics, Advances in Geophysics,* Vol. 28, B. Saltzman, Ed., Academic Press.

——, and L. J. Umscheid, 1987: Comprehensive modeling of the middle atmosphere: The influence of horizontal resolution. *Transport Processes in the Middle Atmosphere,* G. Visconti and R. R. Garcia, Eds., D. Reidel, 251–266.

Manney, G. L., and Coauthors, 1993: The evolution of ozone observed by UARS MLS in the 1992 late winter southern polar vortex. *Geophys. Res. Lett.,* **20,** 1279–1283.

McCormick, M. P., and R. E. Veiga, 1992: SAGE II measurements of early Pinatubo aerosols. *Geophys. Res. Lett.,* **19,** 155–158.

McIntyre, M. E., 1992: Atmospheric dynamics: Some fundamentals with observational implications. *Proc. International School of Physics "Enrico Fermi," CXV Course,* J. C. Gille and G. Visconti, Eds., 313–386.

——, and T. N. Palmer, 1983: Breaking planetary waves in the stratosphere. *Nature,* **305,** 593–600.

——, and ——, 1984: The "surf zone" in the stratosphere. *J. Atmos. Terr. Phys.,* **46,** 825–849.

——, and ——, 1985: A note on the general concept of wave breaking for Rossby and gravity waves. *Pure Appl. Geophys.,* **123,** 964–975.

Murphy, D. M., and Coauthors, 1993: Reactive nitrogen and its correlation with ozone in the lower stratosphere and upper troposphere. *J. Geophys. Res.,* **98**(D5), 8751–8773.

Norton, W. A., 1994: Breaking Rossby waves in a model stratosphere diagnosed by a vortex-following coordinate system and a contour advection technique. *J. Atmos. Sci.,* **51,** 654–673.

O'Sullivan, D., and M. L. Salby, 1990: Coupling of the quasi-biennial oscillation and the extratropical circulation in the stratosphere through planetary wave transport. *J. Atmos. Sci.,* **47,** 650–673.

Pierce, B. R., and T. D. A. Fairlie, 1993: Chaotic advection in the stratosphere: Implications for the dispersal of chemically perturbed air from the polar vortex. *J. Geophys. Res.,* **98,** 18 589–18 598.

——, W. T. Blackshear, T. D. A. Fairlie, W. L. Grose, and R. E. Turner, 1993: The interaction of radiative and dynamical processes during a simulated sudden stratospheric warming. *J. Atmos. Sci.*, **50,** 3829–3851.

Plumb, R. A., D. W. Waugh, R. J. Atkinson, M. R. Schoeberl, L. R. Lait, P. A. Newman, E. V. Browell, A. Simmons, M. Loewenstein, D. W. Toohey, and L. M. Avallone, 1994: Intrusions into the lower stratospheric arctic vortex during the winter of 1991/92. *J. Geophys. Res.*, **99,** 1089–1106.

Polvani, L. M., and R. A. Plumb, 1992: Rossby wave breaking, microbreaking, filamentation and secondary vortex formation: The dynamics of a perturbed vortex. *J. Atmos. Sci.*, **49,** 462–476.

Randel, W. J., J. C. Gille, A. E. Roche, J. B. Kumer, J. L. Mergenthaler, J. W. Waters, and E. F. Fishbein, 1993: Planetary wave mixing in the subtropical stratosphere observed in UARS constituent data. *Nature*, **365,** 533–535.

Read, W. G., L. Froidevau, and J. W. Waters, 1993: Microwave limb sounder measurement of stratospheric $SO_2$ from the Mt. Pinatubo volcano. *Geophys. Res. Lett.* **20,** 1299–1302.

Salby, M. L., D. O'Sullivan, R. R. Garcia, and P. Callaghan, 1990a: Air motion accompanying the development of a planetary wave critical layer. *J. Atmos. Sci.*, **47,** 1179–1203.

——, R. R. Garcia, D. O'Sullivan, and P. Callaghan, 1990b: The interaction of horizontal eddy transport and thermal drive in the stratosphere. *J. Atmos. Sci.*, **47,** 1647–1665.

——, ——, ——, and J. Tribbia, 1990c: Global transport calculations with an equivalent barotropic system. *J. Atmos. Sci.*, **47,** 188–214.

Trepte, C. R., and M. H. Hitchman, 1992: Tropical stratospheric circulation deduced from satellite aerosol data. *Nature*, **355,** 626–628.

——, R. E. Veiga, and M. P. McCormick, 1993: The poleward dispersal of Mt. Pinatubo volcanic aerosol. *J. Geophys. Res.*, **98,** 18 563–18 574.

Waugh, D. W., 1992: The efficiency of symmetric vortex merger. *Phys. Fluid A*, **4,** 1745–1758.

——, 1993a: Contour surgery simulations of a forced polar vortex. *J. Atmos. Sci.*, **50,** 714–730.

——, 1993b: Subtropical stratospheric mixing linked to disturbance of the polar vortices. *Nature*, **365,** 535–537.

——, and R. A. Plumb, 1994: Contour advection with surgery: A technique for investigating finescale structure in tracer transport. *J. Atmos. Sci.*, **51,** 530–540.

——, ——, R. J. Atkinson, M. R. Schoeberl, L. R. Lait, P. A. Newman, M. Loewenstein, D. W. Toohey, L. M. Avallone, C. R. Webster, and R. D. May, 1994a: Transport of material out of the stratospheric Arctic vortex by Rossby wave breaking. *J. Geophys. Res.*, **99,** 1071–1088.

——, L. M. Polvani, and R. A. Plumb, 1994b: Nonlinear, barotropic response to a localized topographic forcing: Formation of a "tropical surf zone" and its effect on interhemispheric propagation. *J. Atmos. Sci.*, **51,** 1401–1416.

Yoden, S., and K. Ishioka, 1993: A numerical experiment on the breakdown of a polar vortex due to forced Rossby waves. *J. Meteor. Soc. Japan*, **71,** 59–72.